Strength and Ductility of HPS70W Tension Members and Tension Flanges with Holes

by

Robert J. Dexter, Steven A. Alttstadt, and Christopher A. Gardner

University of Minnesota

122 CivE, 500 Pillsbury Dr. S.E.

Minneapolis, MN 55455-0116

March 2002

Sponsors:

U.S. Department of Transportation
Federal Highway Administration

American Iron and Steel Institute

High Performance Steel Task Group

PDM BRIDGE

Bethlehem

Acknowledgements

The authors are grateful for the funding provided by PSI, the contractor providing services to Turner-Fairbank Highway Research Center of the Federal Highway Administration (FHWA). William Wright of FHWA was the technical monitor and Mohammad Khan of PSI was the contract monitor.

The research was part of the interagency High Performance Steel (HPS) project, a cooperative research program involving the American Iron and Steel Institute (AISI), the Federal Highway Administration (FHWA), and the Naval Surface Warfare Center (NSWC). The AISI steel bridge task force leads the project, in close cooperation with the AASHTO T-14 Committee (Steel Bridges). This project was part of the research conducted by the HPS Design Advisory Group of the steel bridge task force. In particular, the authors would also like to thank Camille Rubeiz, Director, Transportation and Infrastructure, AISI, Dennis Mertz, Chairman of the HPS Design Advisory Group, and Edward Wasserman, Chairman of AASHTO T-14 Committee.

AISI also provided a supplemental grant for student support. The steel was donated by Bethlehem Steel Corporation and the test specimens were fabricated at no cost by PDM Bridge in Eau Claire, Wisconsin.

The authors would also like to thank Paul M. Bergson for oversight of and assistance with the experimental work in the Structural Laboratory at the University of Minnesota.

Abstract

Experimental and analytical research was conducted to determine the strength and ductility performance of tension members and the tension flange of flexural members fabricated with HPS70W steel and to examine the applicability of current AASHTO tension-member and tension-flange design specifications for HPS70W. Wide-plate tests were conducted to investigate the behavior of members with a variety of net-sections (A_n) due to one or more holes that reduced the gross-section area (A_g) and to compare the HPS70W to HPS100W and ordinary Grade 50 steel. These tests were also simulated using elastoplastic shell finite-element analyses. HPS70W tensile ductility capacity is well within required ranges for structural steel and performed well in these experiments. It was confirmed that the yield-to-tensile strength ratio (Y/T) was a key parameter determining the ductility, and that the behavior of all grades of steel could be predicted based on the ratio $(A_n/A_g)/(Y/T)$. More than adequate ductility is provided at $(A_n/A_g)/(Y/T)$ ratio of 1.0. A three-point bending test of a large-scale girder demonstrated the good performance of the tension flange in flexure and provided a link to the tests on tension members. Recommendations are made for improved design provisions for tension flanges with holes.

Table of Contents

1.0 Introduction

An experimental and analytical research program was conducted to investigate the strength and ductility of steel tension members and the tension flanges of steel flexural members. The primary objectives of this investigation were to determine the adequacy of the tensile ductility of HPS70W steel and to evaluate the applicability to HPS70W steel of current AASHTO tension-member and tension-flange design provisions, which were developed primarily on the basis of tests on components fabricated from mild steel. HPS70W is a "high-performance steel" meaning that it has higher strength (a minimum specified yield strength (MSYS) of 70 ksi) while also having higher fracture toughness, better weldability, and other improved properties relative to conventional bridge steel with a MSYS of 50 ksi or less.

There are concerns, however, about the ductility of any high-strength steel that stem primarily from a tests by McDermott (1969) on girders made of A514 steel (MSYS of 100 ksi). These girders had predicted failure modes of either local or lateral buckling of the compression flange. Two of these girders unexpectedly experienced premature necking on the tension flange, shortly followed by complete tension flange fracture. This behavior was attributed to inadequate strain hardening of the A514 steel.

The strain hardening potential of steel is often characterized in terms of the yield to tensile strength ratio (Y/T), and A514 steel has an average Y/T of about 0.94 (Brockenbrough 1995). The average Y/T for HPS70W is about 0.84, which is greater than the Y/T for conventional Grade 50 bridge steel (typically about 0.77). Because of the variability, the Y/T for HPS70W can range as high as the values for A514 steel in some cases, hence the concern about the tensile ductility of this steel also. Although not discussed by McDermott, the A514 steel of that time often had poor fracture toughness, so this could also have been a factor in

the observed premature tension flange failures in his experiments. Since HPS70W steel has extraordinary fracture toughness, this would not be a factor for HSP70W girders.

A study by Kulak and Fisher (1969) of A514 bolted splice connections in tension members noted a finding related to McDermott's study. Kulak and Fisher observed premature localization of yielding and fracture on the net sections of bolted joints when the A_n/A_g was less than the Y/T of the A514 steel.

The primary emphasis of the testing and analysis in this first phase of this research project was tension members, which were simulated using wide-plate specimens. The cross section of the wide-plate specimen was 8 inch wide by 0.75 inch thick. Wide-plate tests were performed with various net-section areas (A_n) due to one or more holes that reduced the gross-section area (A_g). The tensile ductility of the HPS70W specimens was compared to results from identical specimens of A709 Grade 50 steel, with greater strain hardening and presumably greater ductility, and HPS100W, with a less strain hardening and presumably less ductility.

It was found that HPS70W performed well in these experiments and that the tensile ductility capacity is well within required ranges for structural steel. The controlling factor in ductility of these tensile members was shown to be ratio of the (A_n/A_g) ratio to the Y/T ratio ((A_n/A_g) / (Y/T)). This ratio can also be thought of as the ratio of the nominal fracture limit-state (A_n*T) to the nominal gross-section yielding limit-state (A_g*Y). More than adequate ductility is provided at (A_n/A_g)/(Y/T) ratio of 1.0, although the ductility increases sharply as this ratio exceeds 1.1 (as the fracture limit-state exceeds the gross-section yielding limit state).

A single HPS70W girder test was also conducted in this first phase of the research. This test demonstrated that HPS70W did not exhibit premature necking or inadequate tensile

ductility in flexure, in this one case. More girders will be tested in a second phase of this research to more fully investigate the behavior of tension flanges of HPS70W girders under a range of conditions.

In addition, the statistical variation of Y/T was studied to determine adequate margins of safety to use in design equations when all that is known is the ratio of the minimum specified values of yield strength and tensile strength (F_y /F_u) rather than the actual Y/T. Recommendations are made for improved AASHTO provisions for tension flanges with holes.

1.1 High-performance steel

High Performance Steel (HPS) is a term that is sometimes used to describe a range of high-strength low-alloy (HSLA) steels. These HPS have very low carbon content (less than 0.01%) and typically get their higher yield strength, 65 ksi or greater, from some kind of thermal and/or mechanical processing; including:

1) quenching and tempering (Q&T),
2) precipitation hardening (PH)
3) controlled rolling (CR),
4) combined controlled rolling with accelerated cooling (water spraying), known as thermo-mechanical controlled processing (TMCP).

Primarily because of the reduced carbon, HPS typically have excellent weldability (resistance to hydrogen cracking) and fracture toughness, especially in comparison to traditional high-strength steels that get their strength from the hardenability of carbon and other alloys. Because of these advantages, the higher strength, and other advantages, HPS have been widely used since the 1980's in military ships, gas transmission pipelines, offshore structures, and other demanding applications.

If the size of the market for HPS could be expanded to include civil infrastructure and other applications, the steel could be produced more affordably. Therefore, in 1994, a cooperative research program involving the American Iron and Steel Institute (AISI), the Federal Highway Administration (FHWA), and the Naval Surface Warfare Center (NSWC) led to the introduction of a specific type of High Performance Steel (HPS), which can now be specified as ASTM A709 Grade HPS70W, or, equivalently, as AASHTO M270 Grade

HPS70W. Today, what was once a more general term, HPS, will be used to refer to this specific type of bridge steel.

HPS70W has minimum specified yield strength (MSYS) of 70 ksi. In addition to higher strength, HPS70W offers enhanced weathering properties, increased weldability, and increased fracture toughness. The cost advantages of HPS70W have now been demonstrated in bridge projects in many states, particularly Nebraska, Tennessee, New York and Pennsylvania.

As with all new and innovative structural materials, however, an experimental base must be established for HPS70W and other similar low-carbon HSLA steels. The applicability of current codes and specifications to the new steel must be evaluated and if necessary, new specification provisions should be recommended. To this end, Wright et al (2001) has characterized fracture behavior of HPS70W plate girders and obtained fracture toughness data for HPS70W. Weldability and hydrogen-induced-cracking studies have been performed at LeTourneau University.

1.2 Review of HPS70W flexural test data

The focus on much of the experimental and numerical research studies of HPS70W so far has been on the flexural capacity and ductility of compact and non-compact bare steel HPS plate girders (White and Barth, 1998; Yakel, Mans, Azizinamini, 1999; Green et al, 2000; Barth 2000; Fahnstock 2000; Yakel 2002). The ductility is governed by the compression flange local buckling limit state, as would occur in positive bending during unshored construction or at the piers in the negative moment region of continuous girders.

AASHTO Specifications limit non-compact girders (slender compression flange) to yield moment capacity while compact sections may reach their plastic moment strength. Sections that are compact and satisfy more stringent bracing requirements are also allowed some inelastic moment redistribution, i.e. 10% of the maximum elastic pier moments can be redistributed to positive bending moment.

A standard measure of ductility for flexural members is the inelastic rotational ductility. To illustrate the computation of the rotational ductility, the girder test performed in this research will be briefly described, although details of the test and the results are described further in Section 2.3. The asymmetric girder, shown in Figure 1.1, was proportioned with a very thick (8-inch wide by 3.5-inch thick) compression flange in order to get the location of the neutral axis at the top of the web. The high neutral axis location was intended to simulate the positive moment flexural behavior of a composite section and associated high strain demand in the tension flange.

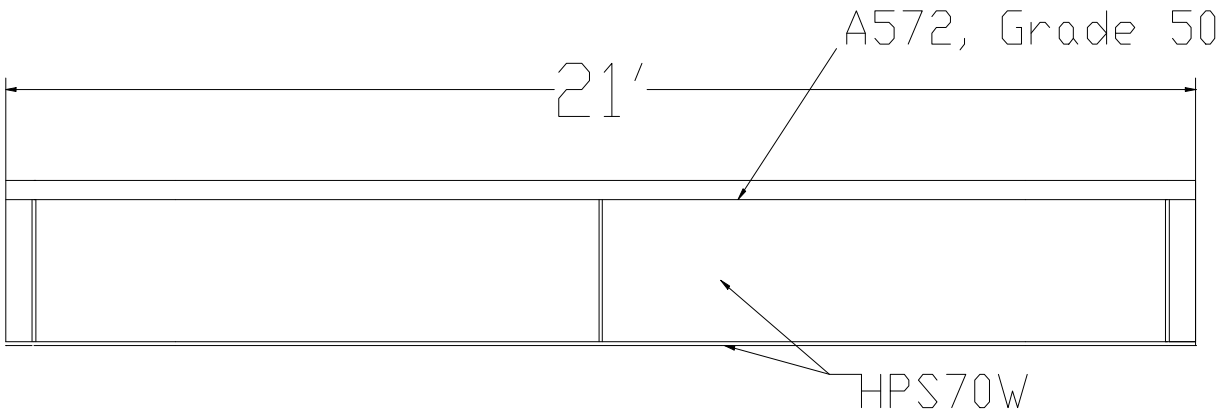

Figure 1.1 - Large-scale girder test specimen geometry

In order to maximize the tensile strain demand, the girder was designed to suppress web buckling, local flange buckling, and lateral torsional buckling. The girder was tested in three-point bending on a 20-foot span. The HPS-70W tension flange was 8-inches wide and 0.75-inches thick, the same cross section as the wide-plate test specimens. The web was 26 inches deep, giving an overall depth of 30.25 inches.

Rotation angles were measured at the end of the girder and deflection was measured at the center of the girder, from which an estimate of the rotation at the center of the girder was obtained. Rotation angles at the end and at the center of the girder are illustrated in Figure 1.2.

Figure 1.2 – Definition of rotation angles at the end and at the center of a beam

Figure 1.3 shows the moment vs. end rotation curve for the HPS70W girder test performed in this research project. The plastic moment capacity of the girder (2950 ft-kips) is shown as a horizontal dotted line. An estimate of the rotation corresponding to the plastic moment is used to separate the plastic deformation from the elastic deformation. Identification of the experimentally measured rotation at the proportional limit or at the point where the plastic moment is reached is difficult and imprecise. Therefore, an easily calculated quantity, the elastic rotation, is used as a reference rotation. The elastic rotation (Θ_y) is the elastically calculated rotation corresponding to an elastic moment equal to the plastic moment capacity. In Figure 1.3, Θ_y is equal to 2.34% radians and this is shown as a vertical dotted line.

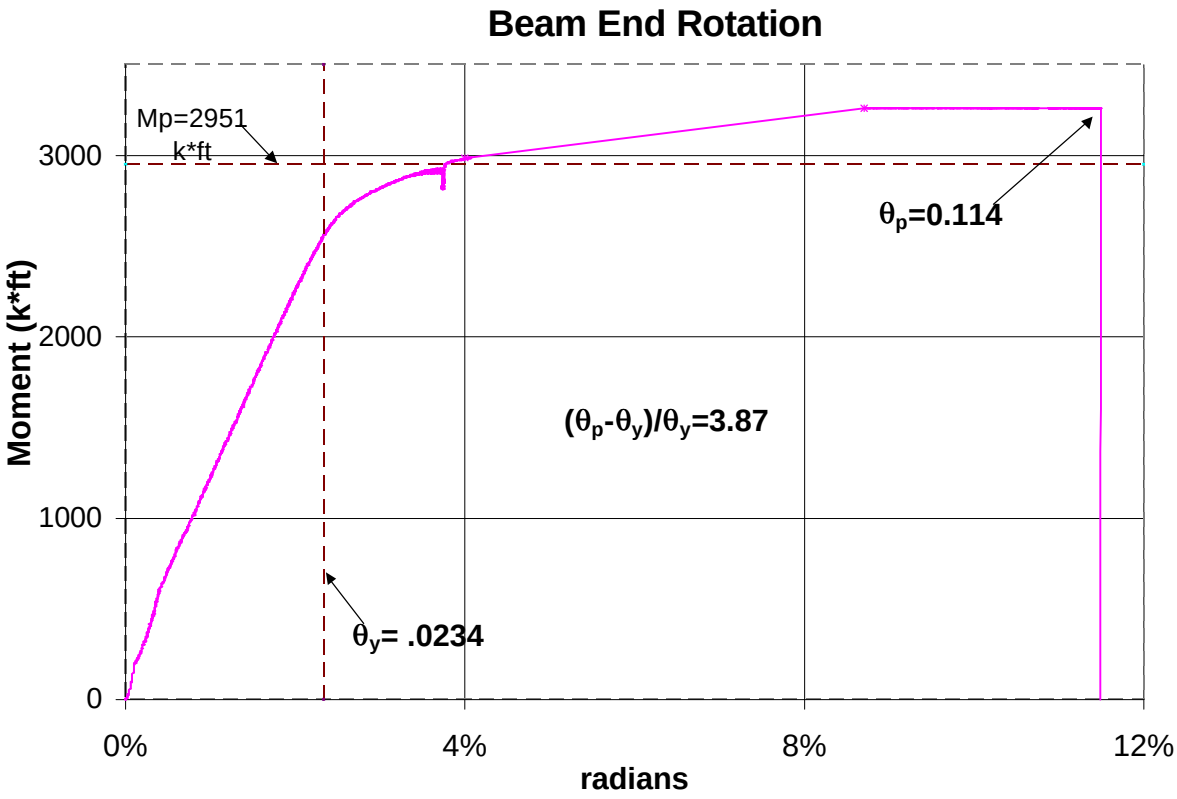

Figure 1.3 - Moment rotation curve for three-point bending test of HPS70W girder

The maximum plastic rotation (Θ_p) is the rotation at failure or at the point when the moment rotation curve crosses back below the plastic moment capacity. In the case of this girder test (the data shown in Figure 1.3), the girder failed suddenly and catastrophically by lateral-torsional buckling at a rotation of about 11.4% before it crossed back below the plastic moment capacity.

The rotational ductility (R) is calculated as follows (Lukey and Adams 1969):

$$R = \frac{(q_p - q_y)}{q_y} \qquad \text{Eq. 1.1}$$

From the data in Figure 1.3, the rotational ductility for this HPS70W girder was about 3.9.

A specific level of rotational ductility (i.e. R = 3) has been established as sufficient to allow girders and beams to allow for some inelastic moment redistribution in flexure (Galambos, et al, 1997). Because of concerns that high-strength steels cannot provide this rotational ductility, AASHTO has historically limited the strength of sections with MSYS greater than 65 ksi to the yield moment.

The recent studies of negative bending of HPS70W (White and Barth, 1998; Yakel, Mans, Azizinamini, 1999; Green et al, 2000; Barth 2000; Fahnstock 2000; Yakel 2002) show that compact HPS70W plate girders are able to develop their plastic moment capacity but are not able to provide rotational ductility of 3 in negative bending. As a result, the 10% redistribution provisions stated in section 6.10.4.4 of the AASHTO LRFD Bridge Design Specification and the inelastic methods of analysis as stated in section 6.10.10 should not be used in with HPS70W plate girders. These recommendations are now reflected in the 2000 interim version of the LRFD Specifications. Similar finings were found at Lehigh University for plate girders made with HPS100W (MSYS of 100 ksi) (Fahnstock 2000).

As demonstrated in the A514 girder tests of McDermott (1969) discussed above, it is also possible that the tension flange could limit the rotational capacity of a girder, especially in the positive moment regions. Therefore, specific levels of tensile flange ductility are also required for girders and also for tension members. Tension flange or tension member ductility may be limited by brittle fracture, necking and tensile rupture in the gross section, or, if there are any holes in the cross section, by tensile rupture on the net section (so called net-section fracture).

Experimental work assessing the tension flange ductility of HPS70W is very limited. Before the girder test performed in this study (the results in Figure 1.3), two composite girder

tests were conducted at University of Nebraska – Lincoln (Mans 2002). One of the specimens was designed to maximize the strain in the tension flange -- 1.2% strain was measured before crushing of the concrete. The strain in the girder test performed in this study exceeded 6%, in comparison. Therefore this test created extremely large tensile flange ductility demand, far in excess of what would typically be experienced in a typical bridge girder in either positive or negative bending.

1.3 Relationship of strain hardening to tensile ductility

The tensile ductility is limited by the strain at which necking begins. Theoretically, it can be shown that there is a connection between the strain at which necking begins (also the point of ultimate strength in a tension test) and the strain hardening of the steel. The theoretical connection can be shown for the case when the inelastic region of a stress–strain curve is represented by a power law:

$$s_{True} = Ke^{n}_{Natural} \qquad \text{Eq. 1.2}$$

where K is the strength coefficient and n is the strain-hardening exponent. It can be shown that the necking strain is equal to the strain-hardening exponent, n (Ripling and Polakowsky, 1966).

Steel such as A514 steel, with a high Y/T that may exceed 0.9, may have a strain hardening exponent as low as 0.08 (indicating that necking could start prematurely at about 8% strain). Ordinary Grade 50 steel, with low Y/T less than 0.8, have a strain hardening exponent on the order of 0.2 (indicating that necking will not start until 20% strain).

Therefore, the elevated Y/T ratio of high-strength steels could result in a dramatic reduction in their tensile ductility and associated rotation capacity. It is oversimplifying, however, to idealize the stress-strain curve as a power law or to characterize the tensile behavior with a single parameter (Y/T). Each steel grade has a different shape of the stress-strain curve (Brockenbrough 1995). It is difficult to isolate the individual effects of an upper yield point, length of the yield plateau, slope of the stress-strain curve in the inelastic range, etc.

1.4 Design specification provisions

The various specification provisions for tension members and tension flanges of flexural members are discussed next, especially the specification provisions that affect ductility. In the AASHTO specifications for bridges, tensile ductility is assured by limiting the selection of structural steels to those included in AASHTO material specifications for bridge steels. These specifications were developed over the years to guarantee that bridge steel would provide good fracture toughness and elongation.

The second, more explicit, provision of adequate ductility is through design requirements. Although the design provisions for bridge girders appear to be primarily focused on strength alone, many of the provisions are intended to provide adequate ductility as well as strength. For example, Section 6.10.4.2.2 of the AASHTO LRFD Bridge Design Specifications requires a check on the plastic neutral axis location for composite plate girders in positive bending to assure that the steel yields significantly before concrete crushing occurs.

There are also explicit specification provisions that account for the effect of holes in the tension flanges of girders on the flexural capacity. These provisions prevent net-section fracture of the tension flange. Since net section fracture is not a concern in compression, there is no limit on the flexural capacity due to holes in the compression flange. Also, the net section does not need to be taken onto account for deflection calculations, which can be based on the gross-section moment of inertia. The additional elastic curvature that occurs at the net section by virtue of the reduced moment of inertia occurs only over a very short length, and therefore it does not contribute significantly to the deflection.

If there is localization of the plastic strain on the net-section without significant plastic strain occurring on the gross section away from the net section, this will lead to a net-section fracture in a girder tension flange. In this case, or if there is premature necking of the gross section of the tension flange, the deformation and associated increase in curvature is localized and only extends over a short length. There is little additional global rotation, which is the integral of the curvature over the length. This observation is analogous to the observation that in a tensile test, there is little additional elongation (when the elongation is expressed as a percentage of the gage length) after necking starts, since the additional straining takes place over a necking length which is much shorter than the gage length.

Therefore, in order to develop adequate rotational capacity for girders, it is essential to avoid the limit state of net-section fracture of the tension flange. This is often accomplished by limiting the applied moment on the cross section with the holes so the axial force in the tension flange is much less than the net-section fracture capacity. For example, splice connections in continuous girders are often located at the points of dead-load contraflexure, where the moment demand is very small relative to the net section flexural capacity. To be conservative, the net section flexural capacity is computed in terms of the yield moment on the net section.

Even if the net-section fracture limit state is to be avoided, an estimate of the net-section capacity is required. As mentioned previously, it is usually accepted that the yield moment computed using the elastic section modulus based on the flange net area can always be attained. However, it is not clear that in all circumstances that a flange net section can reach the limit state of the ultimate strength on the net section. When there are holes in the flange, there is a stress concentration factor of 3 at the edge of the hole. Therefore, the

material immediately adjacent to the holes begins yielding at a much lower load level and must absorb considerable strain in order to develop the limit state of ultimate tensile strength across the net section.

However, it is not always possible to locate holes in tension flanges in areas of low moment demand. There may be holes in the tension flange near points of maximum moment demand. Holes may be for miscellaneous details such as for angle connections between connection plates and flanges (some states are reluctant to weld connection plates to the tension flange), for bridge-mounted signs, or for fall protection during erection. If these holes are sufficiently small, they should not affect the moment capacity, i.e. that the plastic moment capacity on the gross section can still be reached.

Traditionally, in various steel design specifications, no reduction in the moment capacity (relative to the plastic or elastic moment capacity of the gross section) was required if the ratio of the net section area of the tension flange to the gross area of the flange (A_n/A_g) was greater than 0.85. This rule has been referred to as the 15% rule, since the holes can be up to 15% of the original flange gross area. If the A_n/A_g was less than 0.85, then the net section area of the flange was used in calculating the section properties and, typically, only the yield moment could be used rather than the plastic moment.

More recently, in Load and Resistance Factor Design (LRFD) specifications, the allowable A_n/A_g is defined in terms of the minimum specified yield and tensile strengths. For example, in the American Institute of Steel Construction (AISC) specifications, Equation B10-1 (shown below as Equation 1.3) says that no reduction in the moment capacity of a flexural member needs to be made for holes in the tension flange if:

$$0.75F_uA_n > 0.9F_yA_g \qquad \text{Eq. 1.3}$$

where: F_u = specified minimum tensile strength of flange (ksi)

F_y = specified minimum yield strength of flange (ksi)

0.75 = AISC resistance factor for net-section fracture of tension members, and

0.9 = AISC resistance factor for flexure and for gross-section yielding of tension members

Equation 1.3 compares two limit states for tension members, assuring that the net-section fracture strength exceeds the gross-section yielding strength, i.e. assuring that net-section fracture will not occur because the gross-section yielding will always occur first, acting like a fuse. In this case, the holes may be ignored and the plastic moment capacity may be calculated using the gross section area of the tension flange for design.

The resistance (or ϕ) factors are for the most part supposed to provide uniform reliability for the various limit states. If this were true, then it would be appropriate to include them in Equation 1.3. However, ϕ for net-section fracture was chosen to achieve much greater reliability than for gross section yielding, because net-section fracture is a relatively undesirable failure mode (Galambos, 1985). Therefore, net-section fracture would not be expected to occur unless the net section was much smaller than implied by Equation 1.3. In other words, Equation 1-3 is very conservative.

Equation 1.3 can be rearranged as:

$$A_n/A_g > (0.9/0.75)\ (F_y/F_u) = \gamma\ (F_y/F_u) \qquad (1.4)$$

where γ is equal to 1.2, which is the ratio of the ϕ factors.. (Note that these AISC ϕ factors are different from the corresponding AASHTO ϕ factors (0.95/0.8) although their ratio is nearly identical, so this does not impact the effect of these provisions.)

As mentioned previously, it was found in the present study that the ductility is very good provided $A_n/A_g > F_y/F_u$, and the ductility increases rapidly as $A_n/A_g > 1.1$ (F_y/F_u). Therefore, this AISC Equation B 10-1 has the right form, although it is not clear if γ needs to be as great as 1.2, i.e. if the ratio of the ϕ factors should be used.

For A36 steel, ($F_y/F_u = 0.62$), AISC Equation B 10-1 would allow holes up to 25% of the cross section to be ignored, which would be more generous than the 15% rule. However, for typical Grade 50 steel ($F_y/F_u = 0.77$), AISC Equation B 10-1 would allow only 8% of the cross section to be removed for holes. Thus, these provisions are clearly much more restrictive than the traditional 15% rule for higher-strength steel. For HPS70W ($F_y/F_u = 0.82$) it is not possible to have any reasonably sized hole and avoid a reduction in the moment capacity.

If the inequality of Equation 1.3 is not satisfied, then the AISC provisions require that the moment capacity be limited to the yield moment on a cross section with the following effective tension flange area:

$$A_e = \frac{5}{6}\frac{F_u}{F_y}A_n \qquad \text{Eq. 1.5}$$

If the stress is limited by using the reduced section modulus based on A_e, then net-section fracture is not possible and need not be explicitly checked. Note that the fraction 5/6 is the inverse of the factor γ in Equation 1.4 or the ratio of the ϕ factors. Equation 1.5 reveals the dependence of this design provision on steel's Y/T value, which is theoretically linked to the material's ductility capacity.

In the AISC provisions, there is a discontinuity in the flexural capacity at the point when the inequality of Equation 1.3 is no longer satisfied. When the inequality is satisfied,

the moment capacity could be as large as the plastic moment capacity of the gross section. At the point when the inequality is not satisfied, the moment capacity drops to the elastic yield moment on the gross section (since A_e is equal to A_g at this point).

For decreasing A_n, Equation 1.5 allows the design to be based on the yield moment while simultaneously insuring that the nominal stress on the net section of the tension flange does not exceed 0.75 F_u. For Grade 36 steel, Equation 1.5 indicates that A_e can be up to 34% greater than A_n. (Obviously, A_e should not be taken as greater than the gross area (A_g)). For Grade 50 steel, A_e is only 8% greater than A_n.

If the ratio of the ϕ factors were not in Equation 1.3 and 1.5, then these equations would insure that the nominal stress on the net section would not exceed F_u rather than 0.75 F_u. In this case, A_e could be 30% greater than A_n for Grade 50 steel. So whether the ratio of the ϕ factors appears in these Equations has an especially significant impact for Grade 50 and higher strength steel.

There is reason to believe that the criterion for net section fracture of a tension flange does not need to be as stringent as the 0.75 F_u criterion for net section fracture of a tension member. The behavior of a tension flange in a girder is much different than the behavior of a tension member, for which the resistance factor of 0.75 was obtained. If a tension member is under fixed load and the stress on the net section reaches the actual tensile strength, then fracture occurs instantly. However, the deformation of a tension flange is limited by the restraint provided by the web and therefore is under a loading state closer to fixed displacement, even if the girder itself is under fixed load. Although the tension flange can carry no additional load, the strain on the net section cannot increase rapidly without a

corresponding localization of strain in the girder web. Therefore, it is possible that the stress in a tension flange can reach F_u without causing instantaneous fracture.

There may even be some reserve capacity since the flexural capacity may continue to increase slightly as a plastic stress distribution spreads over the web. The best possible flexural capacity would be the plastic moment capacity on the net section. It typically requires a strain in the tension flange of between 6 to 10 times the yield strain (1.5 to 2.5% strain for HPS70W) for the plastic moment to develop on a cross section. There is some reason to suspect that this may be possible for compact sections with holes in the tension flange, even if the A_n/A_g ratio is much less than the Y/T ratio. For example, this was observed in girder tests reported by Dexter and Gentilcore (2002) with large cracks in the tension flange. These girders could reach the plastic moment on the remaining uncracked net section, provided they had sufficient fracture toughness.

Therefore, the two key questions to be addressed in the additional girder tests to be performed as part of the second phase of this research are:

1) whether limiting the stress in the tension flange to F_u gives a sufficiently small probability of net-section fracture, or whether the net section stress must be limited to $0.75\ F_u$ as in a tension member; and if F_u is sufficient,
2) whether the tension flange can continue to strain up to 2.5% after reaching a nominal stress on the net section equal to F_u so that the plastic moment on the net section can be attained.

The AASHTO LRFD Specifications do not allow any holes at all if the plastic moment capacity is to be used in design. If there are any holes, the maximum moment capacity is limited to the yield moment. This seems more conservative than the AISC

Specifications, however the designs of bridge girders by the LRFD Specifications are usually governed by a serviceability provision to avoid yielding at an overload condition, therefore the plastic moment capacity is rarely needed.

Section 6.10.3.6 of the AASHTO LRFD Specifications require calculation of an effective flange area. As shown in Equation 1.6 below, this effective flange area is calculated as a combination of the net area of the flange plus a factor β times the gross area of the flange.

$$A_e = A_n + \beta A_g \leq A_g \qquad \text{Eq. 1.6}$$

in which:

$$\beta = (A_n/A_g)\,[\,\phi_u F_u / \phi_y F_y - 1\,] \geq 0.0$$

where in the AASHTO Specifications:

ϕ_u = resistance factor for net-section fracture of a tension member = 0.80

ϕ_y = resistance factor for gross--section yielding of a tension member = 0.95

Note that the factor β is analogous to the fraction of the gross area below which the holes must be taken into account when computing the yield moment. Thus, β is somewhat analogous to the old 15% rule, but the rule is now a function of the net and gross areas and the materials yield and tensile strengths.

The AASHTO LRFD Specification Section 6.10.3.6 has also had a limitation on the maximum diameter of the hole, 1.25 inches, above which the factor β must be taken as zero. This limitation is based on the Allowable Stress Design (ASD) Table 10.32.1A in the Standard Specifications, which states that the net section must be used when the holes exceed this diameter. This ASD provision was designed to account for cases not adequately covered when β was a flat 15%. It is presently proposed that this limitation on hole size be removed since β is now explicitly calculated.

Section 6.10.3.6 also explicitly states that the compression flange area may be taken as the gross area, regardless of whether there are holes in the compression flange. The commentary states that net section fracture is not a concern for compression flanges.

Specification 6.10.3.6 can be simplified and shown to be essentially the same as Equation 1.5:

$$A_e = A_n + (A_n/A_g)[\phi_u F_u / \phi_y F_y - 1] A_g$$

$$A_e = A_n + A_n (\phi_u F_u / \phi_y F_y - 1)$$

$$A_e = A_n + A_n (\phi_u F_u / \phi_y F_y) - A_n$$

$$A_e = (\phi_u F_u / \phi_y F_y) A_n$$

$$A_e = (\phi_u / \phi_y) (F_u / F_y) A_n \qquad \text{(Eq. 1.7)}$$

However, in the AASHTO specifications, even if the percentage area of the holes is less than β, the moment capacity must still be limited to the yield moment capacity.

For the AASHTO LRFD Specification, the ratio of the resistance factors results in a factor of 0.84, and that the ratio of F_u/F_y must be less than 0.84 in order for there to be any increase in the effective area above the net area. This factor of 0.84 is essentially the same as the 5/6 in Equation 1.5 and the inverse of the factor γ used in Equation 1.4.

Each type of steel has a unique distribution of possible Y/T values and a unique relationship between the mean Y/T and the ratio of the specified values F_u/F_y. For example, Table 1.1 shows some statistics of the Y/T distribution for A514, HPS70W, various Grade 50 steels, and A36 plate. The data are assumed to be normally distributed and therefore the distribution can .be described by the mean and the coefficient of variation (COV). The mean Y/T is a slightly less than but nearly equal to the F_y/F_u ratio for the A36 and Grade 50 steels

while the mean Y/T for A514 and HPS70W is greater than the F_y/F_u ratio. Clearly the specifications should reflect this difference.

Table 1.1: Parameters of Y/T distribution for HPS70W and other structural steels

Steel	specified F_y/F_u	mean Y/T	Coefficient of Variation
*HPS70W	0.82	0.84	0.060
**A36 plate (t > 0.75")	0.62	0.61	0.080
**A572 Gr 50 plate (t >0.5")	0.77	0.72	0.052
**A588 Gr 50 plate (t <2")	0.77	0.74	0.066
***A992 shapes	0.77	0.76	0.040
**A514 plate (t<2.5")	0.87	0.94	0.017

*this study.
**Brockenbrough, 1995
***Dexter et al, 2001

The experimental results presented in Section 2.2 of this report suggest that, if the Y/T is known, γ in Equation 1.4 need not exceed 1.0 (or equivalently that the number 0.84 in Equation 1.5 or 1.7 need not be less than 1.0). However, in design, the Y/T is not known – rather the only thing known is the ratio of the minimum specified values, F_y/F_u. The statistical variation of Y/T was studied in detail in Section 4.3 to determine adequate margins of safety to use in design equations. An upper bound or safe Y/T value was derived for the grades of steel in Table 1.1 including HPS70W steel. The safe Y/T value was compared to the F_y/F_u ratio to compute an appropriate γ factor for proposed improved design equations as an alternative to the ratio of the ϕ factors.

2.0 Experiments and analyses

Tensile experiments were conducted on 8-inch wide 0.75-inch thick plates with various net-section configurations. Plates without holes, with single holes of varying size, with hole groups, and with splice connections were tested. The experiments, described in Section 2.2, were conducted to characterize the effect of the net section on the tensile ductility of HPS70W and compare it to the ductility of similar specimens made with HSP100W and A709 Grade 50 steel.

In addition, one flexural test was also conducted. As discussed previously in Section 1.2, the girder featured a tension flange that was identical in cross section to the tension specimens. There were no holes in the flanges. This test was conducted to compare the behavior of the tension flange to the tension members and to characterize the ductility demand for the tension flange. Details of the results of this test are discussed in Section 2.3.

2.1 Tensile properties of materials

The steel plates used to fabricate the wide-plate tensile specimens were obtained from two different heats of HPS70W from Bethlehem-Lukens Plate. The plate may have been made by either the Quenched and Tempering (QT) process, or Thermo-Mechanical Control Processing (TMCP). Specimens were also made from one heat of A709 Grade 50 and from one heat of HPS100W. These additional materials are meant to represent an upper bound and lower bound for ductility, respectively, and to provide a frame of reference within which to judge the HPS70W results.

The ¾" thick ASTM A709 HPS70W plates tested in this investigation were supplied by Bethlehem-Lukens Plate and were produced in their Burns Harbor Mill. According to ASTM A709, the MSYS for HPS70W is 70 ksi and the specified range of tensile strengths is 85 – 110 ksi. Table 2.1 compares the tensile properties of both HPS70W heats, labeled L and H, according to the mill test report (MTR), measured with conventional 1.5" wide flat tensile specimens, and measured with 8" wide monolithic (i.e. no holes) tensile specimens.

The HPS70W-L wide-plate, average coupon and average MTR values show good agreement and the variation among the two test results is minimal. The yield strength of the HPS70W-H heat appears to be slightly less than the L heat, although one of the MTR results shows higher yield (94.4 ksi) and tensile strength (104 ksi), and also had the highest Y/T (0.90). It is widely believed that the tensile test performed at the mill is typically performed at a strain rate at the upper range of what is allowed under ASTM A370.

Table 2.1 – Comparison of Individual and Average Tensile Test Results

Material	F_y 8" WIDE (ksi)	F_y COUPON (ksi)	F_y MILL (ksi)	F_u 8" WIDE (ksi)	F_u COUPON (ksi)	F_u MILL (ksi)	Y/T 8" WIDE	Y/T COUPON	Y/T MILL
HPS70W-L	**79.95**	81.50 79.50 **80.50**	77.80 79.60 **78.70**	**89.81**	95.00 94.70 **94.85**	89.80 90.00 **89.90**	**0.89**	0.86 0.84 **0.85**	0.87 0.88 **0.88**
HPS70W-H	**76.00**	75.90 75.50 **75.70**	79.90 94.40 **87.15**	**86.89**	92.30 88.80 **90.55**	94.00 104.4 **99.20**	**0.87**	0.82 0.85 **0.84**	0.85 0.90 **0.88**
A709 Gr 50	**60.75**	56.00 52.10 **54.05**	59.00 58.00 **58.50**	**80.99**	82.40 81.30 **81.85**	80.00 79.00 **79.50**	**0.75**	0.68 0.64 **0.66**	0.74 0.73 **0.74**
HPS100W	**115.95**	104.93 103.23 **104.08**	-	**121.33**	109.44 112.34 **110.89**	-	**0.96**	0.96 0.92 **0.94**	-

The ¾" thick A709 Grade 50 plates were supplied by a local distributor. The Grade 50 wide-plate, average coupon and average mill test results showed good agreement. As shown in Table 2.1, the wide plate test had yield strength that was on the high side of the other tests and consequently has a higher Y/T than the coupon tests.

The ¾" thick HPS100W plate tested inthis investigation was donated to the project by the Federal Highway Administration from their Turner-Fairbank Highway Research Center. According to ASTM A709, the MSYS for HPS100W is 100 ksi and the MSTS range is 110 - 130 ksi. Due to limited load capacity of the test machine, 600 kips, the width of the gage length of these specimens was reduced to 6 inches. These details can be material availability,

the wide plate tests for the HPS100W were only 6” wide rather than 8” wide as the other specimens. Table 2.1 provides the tensile properties of the HPS100W plate according to the 6” wide-plate specimen results, and the coupon tests. Mill certifications could not be found for the HPS100W steel plate. The wide plate test shows consistently higher yield and tensile strengths than the coupon tests.

In summary, there is no consistent trend in the differences between the MTR, the coupon tests, and the wide-plate tests. The most likely origin of the differences between these tests is variation of material properties at the different locations in the plate. It is concluded that there is no demonstrable effect of the width of the plates. Therefore, the results of the wide plate tests should be equally applicable to other widths of tension members and flange plates.

2.2 Wide-plate tests

Wide-plate specimens were tested to establish the fundamental behavior of HPS70W tension members before testing more complex flexural members.

2.2.1 Wide-plate specimens

Figure 2.1 shows the basic specimen design. The width of the HPS100W specimens was only 6", due to limited load capacity. A variety of A_n/A_g ratios could be tested simply by adjusting the diameter of the hole in the specimen, including no hole at all for the monolithic tests.

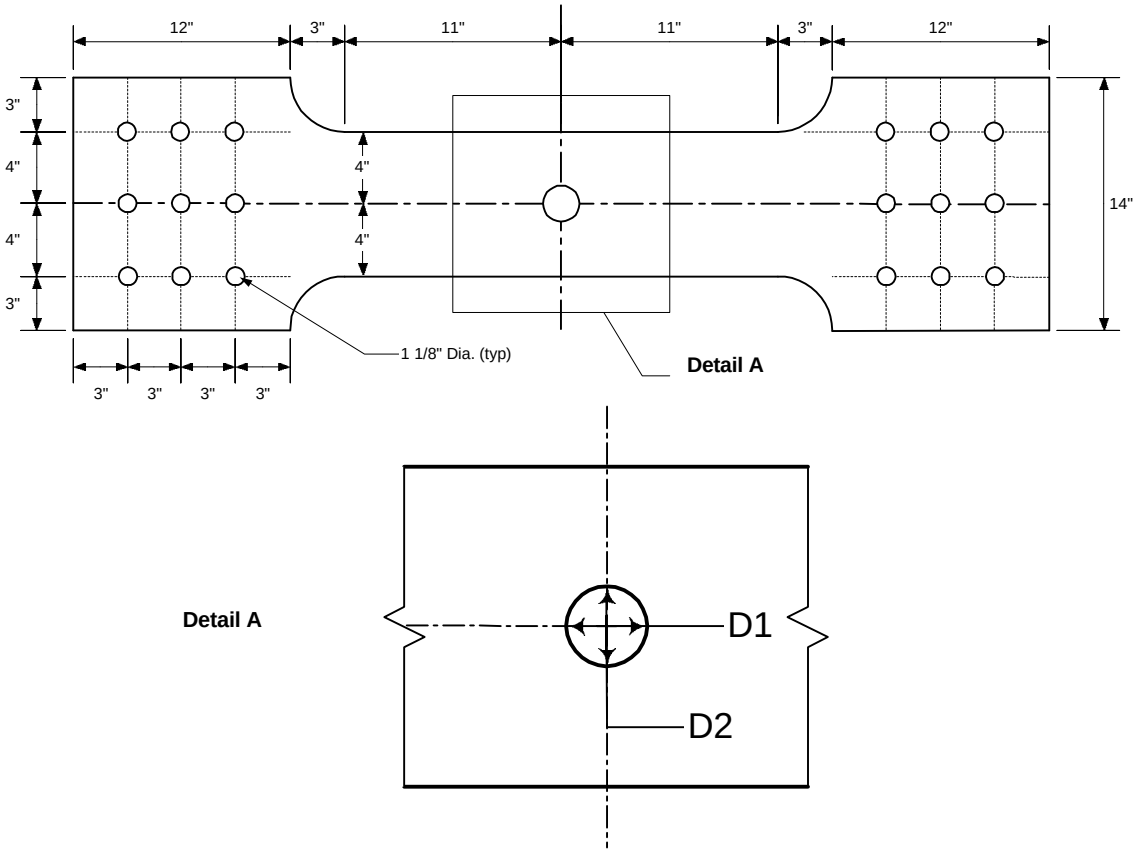

Figure 2.1 – Geometry of Wide-Plate Tension Specimen

The specimens were bolted into grips as shown in Figure 2.2. Nine 1" diameter A 490 bolts were used with a hole diameter of 1.125".

Figure 2.2 – Wide-Plate Tension Specimen in Test Fixture

Specimen identification was based on a combination of steel grade, differentiation between the H and L sample of HPS70W, and the fabricated net section property. This identification system is explained in Figure 2.3. (For the Grade 50 and HPS100W test specimens, there is no H and L because there is only one heat tested.)

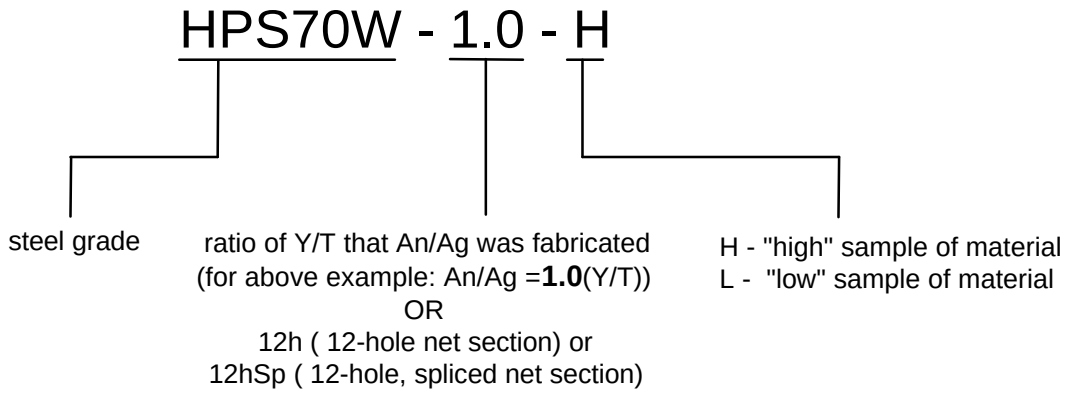

Figure 2.3 – Identification System for Specimens

Six wide-plate tension specimens were flame cut from both the HPS70W-H plate and the HPS70W-L plate. One monolithic specimen, designated as the "0.0" specimen, from each of the HPS70W samples was then tested to failure to find the apparent yield and ultimate strength values for the wide-plate specimen geometry. Based upon these strength results, specimen HPS70W-1.1-H was fabricated by drilling a single, centroidal hole in the gage length of an H and L sample to create an A_n/A_g ratio equal to 1.1(Y/T).

This initial net-section ratio was selected based on the observation that the design specifications require that the A_n/A_g ratio be greater than 1.2(Y/T) to avoid a reduction in moment capacity, and it was anticipated that these specifications would be shown to be too conservative and therefore the specimens with A_n/A_g equal to 1.1(Y/T) should perform well. If not, the A_n/A_g could be increased in the next set of experiments.

As it turned out, the "1.1" specimens, i.e. the specimens with A_n/A_g equal to 1.1(Y/T), did perform well in all cases. Therefore, the additional tests were performed (one for each heat) on "1.0", and "0.9" specimens as shown in Table 2.2.

Table 2.2 – Test Matrix for Monolithic and Single Hole Specimens

Specimen	Design A_n Hole Dia. (in)	Fabricated D1 (in)	Fabricated D2 (in)	Fabricated AVG D (in)	Fabricated A_n/A_g	Fabricated A_n/A_g (Y/T)
HPS70W-0.0-H	0.000	0.000	0.000	0.000	1.000	-
HPS70W-0.0-L	0.000	0.000	0.000	0.000	1.000	-
HPS70W-0.9-H	1.688	1.699	1.696	1.698	0.789	0.902
HPS70W-0.9-L	1.563	1.596	1.569	1.583	0.806	0.905
HPS70W-1.0-H	1.000	1.040	1.031	1.036	0.872	0.997
HPS70W-1.0-L	0.875	0.873	0.882	0.878	0.894	1.004
HPS70W-1.1-H	0.297	0.300	0.299	0.300	0.964	1.102
Gr50-0.0	0.000	0.000	0.000	0.000	1.000	-
Gr50-1.0	2.080	1.996	2.004	2.000	0.750	1.007
Gr50-1.1	1.488	1.404	1.412	1.408	0.824	1.107
HPS100W-0.0	0.000	0.000	0.000	0.000	1.000	-
HPS100W-0.9	0.816	0.827	0.835	0.831	0.862	0.901
HPS100W-1.0a	0.240	0.259	0.273	0.266	0.956	1.000
HPS100W-1.0b	0.240	0.271	0.241	0.256	0.957	1.002

***Y/T Determined from 8" Monolithic Wide-Plate "0.0" Specimen Results**

Because of a limited selection of drill bit sizes, the actual hole size was not exactly that required to achieve the precise ratio of $(A_n/A_g)/(Y/T)$ that was desired. Table 2.2 provides the final fabricated $(A_n/A_g)/(Y/T)$ values in the last column, where the Y/T is that measured in the monolithic "0.0" specimen.

The Y/T value of the HPS100W is so large that the hole size cannot be very large in these specimens, as shown in Figure 2.4 for the specimen where the A_n/A_g was approximately equal to the Y/T. A penny provides scale for the hole size. This illustrates the impracticality of some of the design provisions for holes in tension flanges discussed in the previous section.

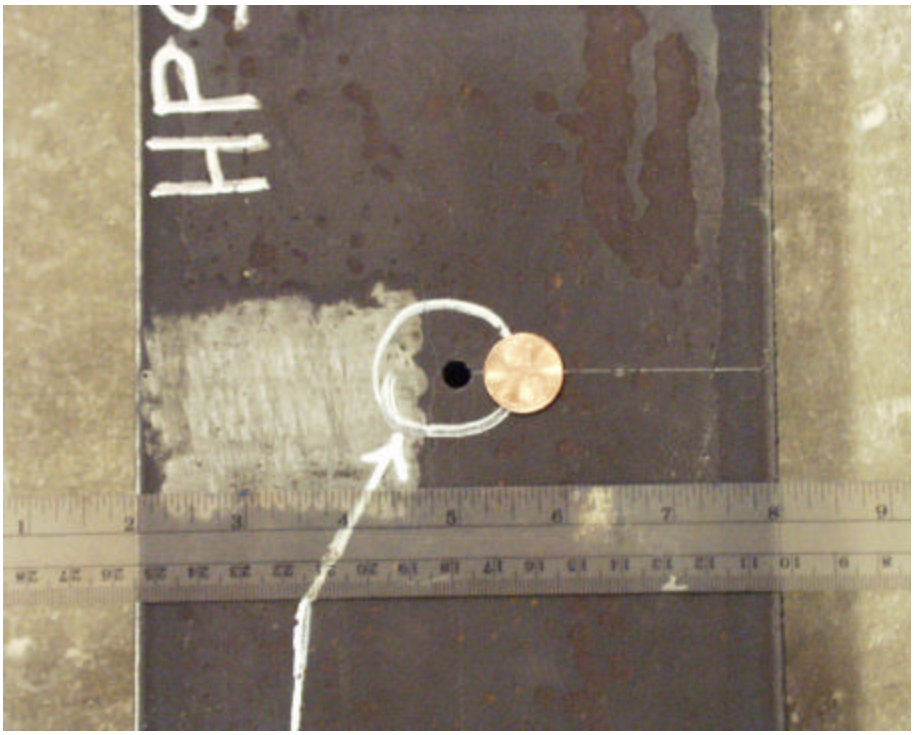

Figure 2.4 – Fabricated Hole Size for HPS100W-1.0(a)

In addition to these specimens with one hole, specimens with 12 holes and specimens with a splice joint were also tested. Figure 2.5 shows the specimen with the splice joint. The cross section of the main plate is the same as the other specimens. The splice plates are also 0.75 inches thick, ensuring the main plate is the critical component.

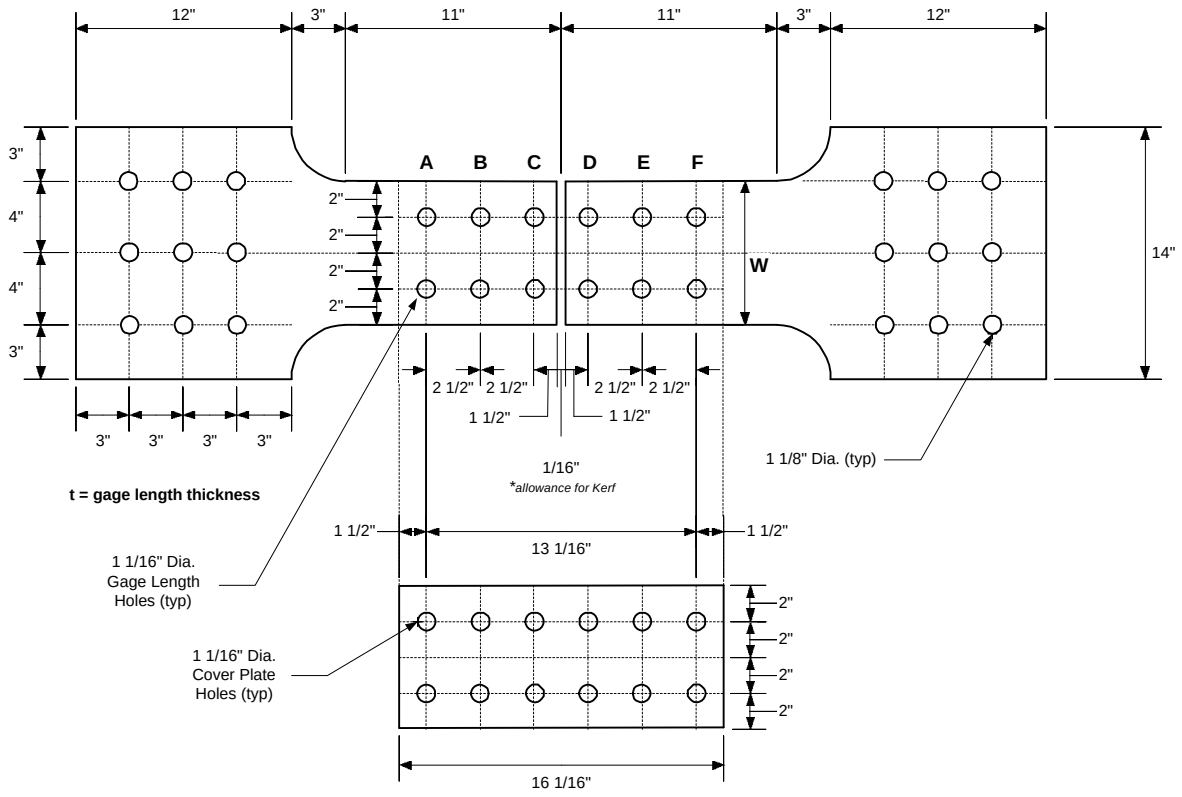

Figure 2.5 – HPS70W Splice Specimen

The test matrix for these splice specimens is shown in Table 2.3. A_n for these specimens is the net-section area of the critical row of holes that experienced fracture during testing. The Y/T from the monolithic wide plates is used to normalize the A_n/A_g ratios in the table.

Table 2.3 – HPS70W 12-Hole Spliced and Unspliced Specimens

Specimen	Design A_n Hole Dia (in)	Avg. Fabricated Hole Dia. Per Cross-Section (in)						Fabricated A_n/A_g	Designed A_n/A_g (xY/T)	Fabricated A_n/A_g (xY/T)
		A	B	C	D	E	F			
HPS70W-12hSp-H	1.063	**1.072**	1.072	1.074	1.090	1.071	1.065	0.732	0.839	0.837
HPS70W-12hSp-L	1.063	1.067	1.071	1.086	1.079	1.079	**1.077**	0.738	0.823	0.829
HPS70W-12h-H	1.063	1.056	**1.053**	1.053	1.053	1.057	1.054	0.743	0.839	0.849
HPS70W-12h-L	1.063	1.062	1.070	1.082	**1.075**	1.075	1.073	0.734	0.823	0.824

Sp indicates spliced specimen
Y/T Determined from 8" Wide-Plate 0.0-H and 0.0-L Specimen Results
Bold diameters indicate the failure plane.

In addition to the bolted specimen tests, it was also decided that an unspliced specimen with the exact same net section properties would be examined. This specimen geometry is presented in Figure 2.6. The bolt hole spacing was identical to the spliced specimens.

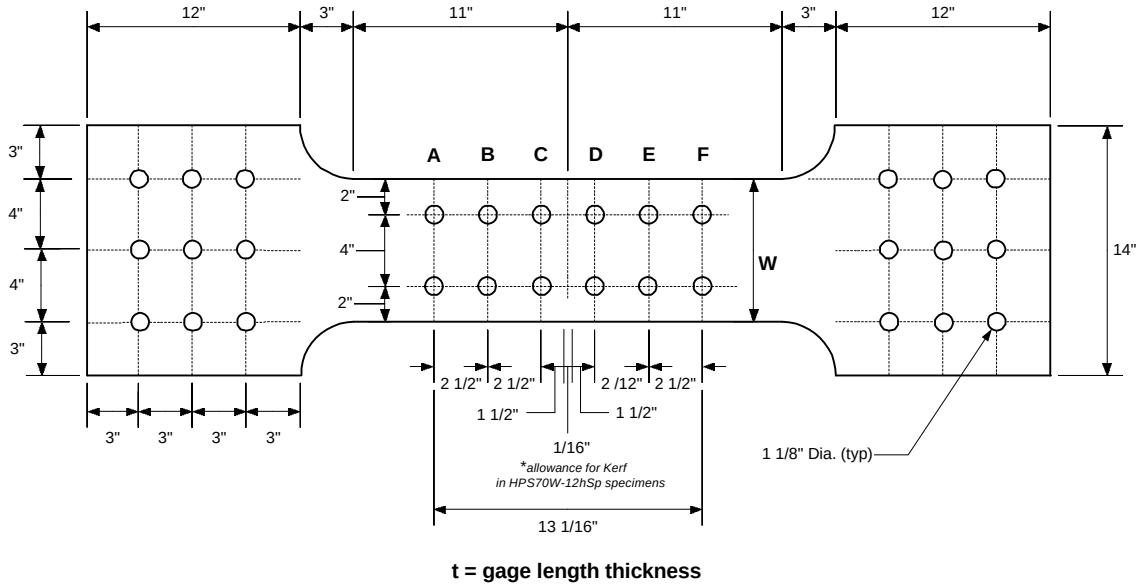

Figure 2.6 – HPS70W 12-Hole Net-Section Specimen

2.2.2 Wide-pate test procedure

In each specimen, strains were measured on the gross section with high-elongation strain gages. In specimens with holes, two high-elongation gages were placed at equal spacing between the edge of the net-section hole and the edge of the plate. Displacement within the gage length was measured with two Linear Variable Differential Transformers (LVDT) – one on the front and one on the back. The gage length for the HPS100W specimens was about 35.5 inches while the gage length for all other specimens was about 26.5 inches. Load and stroke rate were recorded from the universal testing machine.

The effect of strain rate was explored on HPS100W specimens, since this steel had the greatest Y/T. Two HPS100W specimens were tested with $(A_n/A_g)/(Y/T)$ ratios of 1.0. These two tests were conducted at two different strain rates, i.e. 0.16% sec^{-1}.and 0.007% sec^{-1}. This variation had no significant effect on the strength or elongation behavior and therefore these two tests were considered identical in further analysis of the results. All other tests were conducted at an intermediate strain rate of approximately 0.09% sec^{-1}, which corresponds to a test machine crosshead stroke rate of about 0.025 inches/sec

Following installation and instrumentation, an elastic cycle up to half of the yield load was applied to each specimen. The instrumentation was then re-zeroed before the actual test was conducted.

2.2.3 Results of the wide-plate tests

Figures 2.7 and 2.8 show two typical curves of load (normalized by the gross area) and the LVDT elongation (which is the LVDT displacement normalized by the gage length) for specimens HPS70W-0.0-H and HPS70W-1.0-L. The results for each LVDT are shown separately, and it can be seen there is little difference or out-of-plane bending. Therefore, in further discussion, the elongation will be derived from the average of the two LVDT measurements.

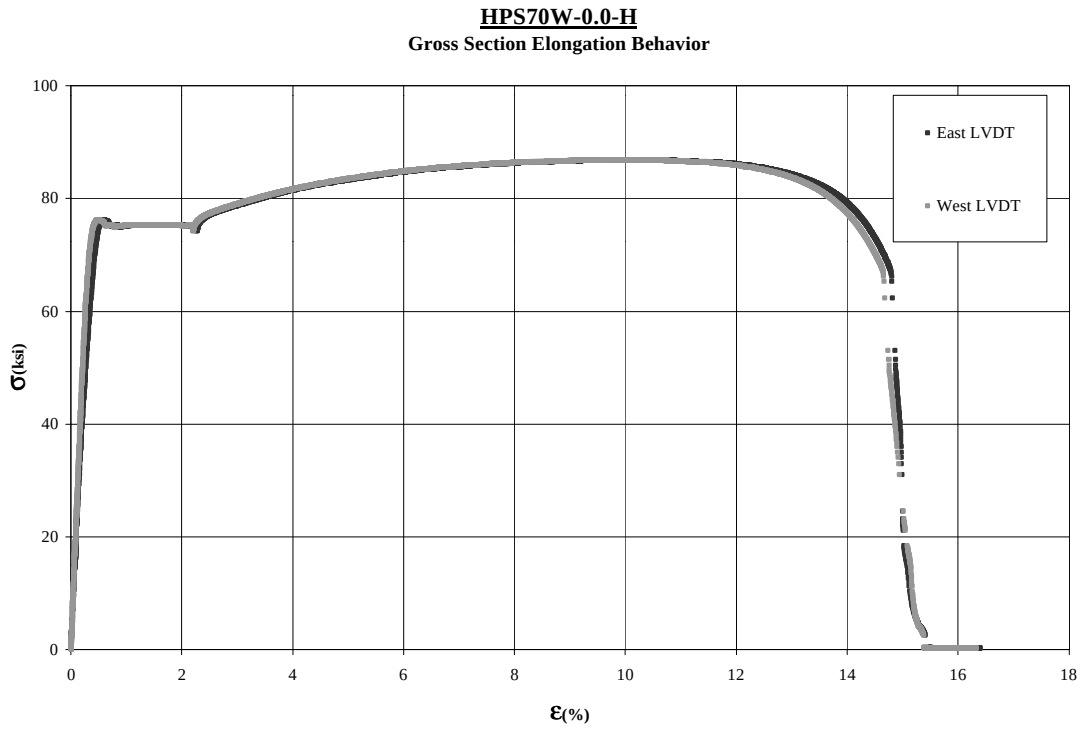

Figure 2.7 – Load vs. elongation for monolithic specimen HPS70W-0.0-H

Figure 2.8 – Load divided by gross section area vs. elongation for HPS70W-1.0-L

In order to define the ductility in a standard way, a scheme for tension members was devised that was analogous to the way flexural ductility is defined, as was shown in Figure 1.3. The yield strain could was defined as the MSYS (70 ksi for HPS870W) divided by the elastic modulus (29,000 ksi), which is about 0.24%.

Alternatively, the apparent proportional limit from each load gross section stress vs. elongation curve could have been used, or the elastic strain corresponding to the yield strength of the particular material could have been used, either from the 8" wide monolithic specimen or from the coupons. It was found that these other definitions of the yield strain caused unexpected variation in the calculated ductility, and more consistent results were obtained when the yield strain was defined in terms of the MSYS.

The maximum elongation (ε_{total}) was defined as the elongation when the nominal stress vs. elongation curve fell below the MSYS, as shown in Figure 2.9. The ductility (R) was then calculated by subtracting the yield strain (ε_y) from the maximum elongation and then dividing the difference by the yield strain, i.e.:

$$R = \frac{\left(e_{total} - e_y \right)}{e_y} \qquad \text{Eq. 2.1}$$

For example, the tensile ductility calculated using this equation for the data in Figure 2.9 is about 37.

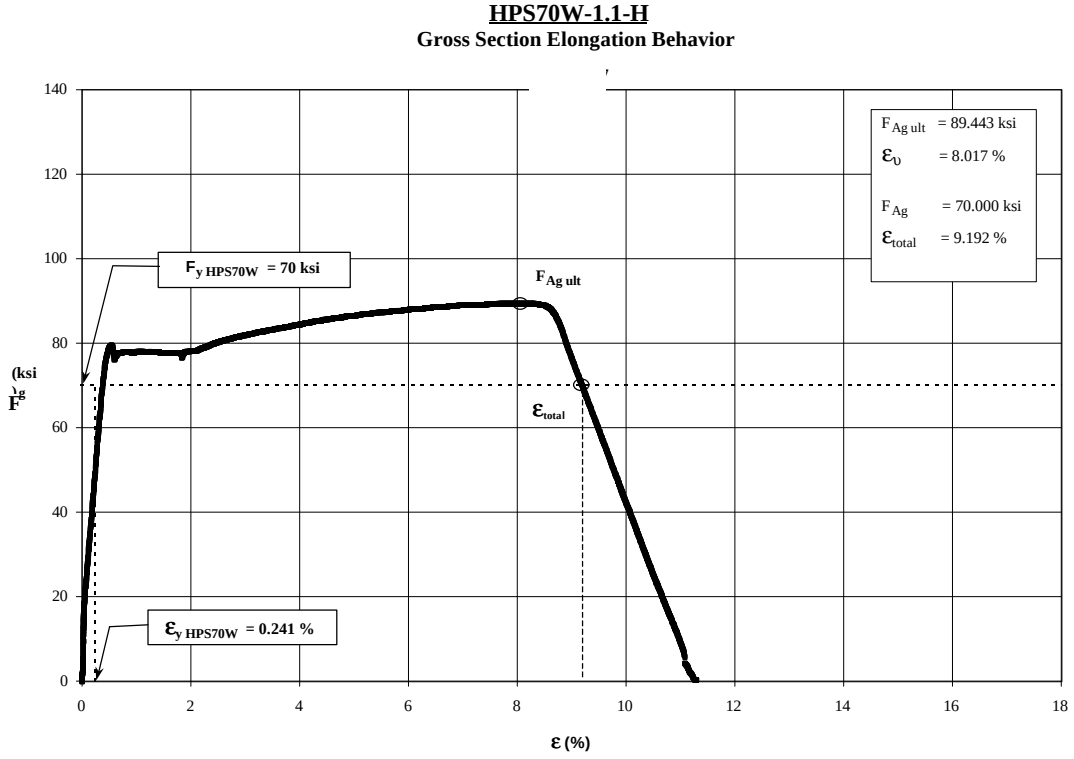

Figure 2.9 – Load divided by gross section area vs. elongation for HPS70W-1.1-H showing maximum elongation and tension ductility

The total elongation quantities for the 12h and 12hSp cases were calculated in a slightly different manner since the gross section stress did not exceed the MSYS. For these cases, an apparent yield point in the gross-section stress vs. elongation behavior was projected horizontally. The point at which the gross-section stress fell below this projection was taken as the total elongation for the specimen.

In addition, for the purposes of comparison with the single-hole specimen data, the total elongation quantities for the HPS70W-12h specimens have been divided by 6 to account for the fact that the localized elongation took place simultaneously on all 6 lines of holes. For the same reason, the HPS70W-12hSp elongation quantities have been divided by 2 to account for the two lines of bolt holes that experienced localized inelastic elongation.

Table 2.4 summarizes the data from the tests on HPS70W. The tensile ductility as defined in Equation 2.1 is given in the last column on the right. Precisely how much tensile ductility is required of a tension flange in order to permit adequate rotational ductility of a girder is not yet clear. For a given level of rotational ductility, the strain demand in the tension flange depends strongly on whether it is positive or negative bending, the depth of the girder, the moment gradient, composite behavior, compactness, and many other factors yet to be quantified for a range of conditions.

For example, the experiments conducted at University of Nebraska – Lincoln (Mans 2002) indicated that the strain in the tension flange was a maximum of 1.2% before crushing of the concrete. Note that every wide-plate specimen tested, even the splice specimens where the A_n/A_g is equal to 0.83 times the Y/T, exhibit at least this much elongation. Given that the yield strain for the MSYS of 70 ksi is 0.24%, this would correspond to a tensile ductility demand of about 4.

Table 2.4 – Summary of HPS70W Wide-plate Tensile Test Results

Specimen	Peak Load (kips)	F_{An} (ksi)	$\frac{F_{An}}{F_u}$	F_{Ag} (ksi)	$\frac{F_{Ag}}{F_y}$	Total Elongation ε_{total} (%)	Net Plastic Elongation $\varepsilon_{plastic}$ (%)	$\frac{\varepsilon_{plastic}}{\varepsilon_y}$
HPS70W-0.0-H	538	86.8	1.00	86.8	1.14	14.59	14.35	59.5
HPS70W-0.0-L	557	89.8	1.00	89.8	1.12	13.34	13.10	54.3
HPS70W-0.9-H	446	91.0	1.05	71.7	0.94	2.38	2.14	8.8
HPS70W-0.9-L	463	93.5	1.04	75.3	0.94	2.72	2.48	10.2
HPS70W-1.0-H	517	94.6	1.09	82.5	1.09	2.72	2.48	10.2
HPS70W-1.0-L	523	92.8	1.03	82.9	1.04	2.94	2.70	11.2
HPS70W-1.1-H	549	92.8	1.07	89.4	1.18	9.19	8.95	37.1
HPS70W-12h-H	423	89.9	1.04	66.8	0.88	6.54	5.10	3.5*
HPS70W-12h-L	431	95.0	1.06	69.7	0.87	6.12	4.68	3.2*
HPS70W-12hSp-H	430	94.1	1.08	68.9	0.91	3.68	3.20	6.6**
HPS70W-12hSp-L	452	97.8	1.09	72.2	0.90	3.60	3.12	6.4**

*tensile ductility divided by 6 for comparison to results with single hole

**tensile ductility divided by 2 for comparison to results with single hole

Analysis of cross sections show that it takes between 6 to 10 times the yield strain in the tension flange, in the case of HPS70W about 1.5 to 2.5% strain, to be able to develop the plastic moment capacity (M_p) of a girder. In the girder test performed in this study (the result shown in Figure 1.3), the strain was about 10 times the yield strain when M_p was first developed. If this were the criterion for tensile ductility, then any specimen where the A_n/A_g was equal to or greater than the Y/T would exhibit sufficient ductility to develop M_p.

At the end of the girder test, the strain in the tension flange exceeded 6%. This girder was proportioned in a very unusual way to maximize the tension flange strain demand, as explained later in Section 2.3, therefore this strain demand should represent an upper bound. Note that only the "1.1 specimen", i.e. the specimen where the A_n/A_g is equal to 1.1 times the Y/T, had sufficient ductility to meet this demanding condition.

Six-percent strain corresponds to tensile ductility demand on this flange of about 24, which corresponded to a rotational ductility of about 3.9. At a rotational ductility demand of 3 for this girder (widely accepted as adequate for plastic redistribution of moments), the tension ductility demand would be about 18. In summary, adequate tensile ductility is somewhere in the range from 6 to 18.

As the loading increased on the single-hole specimens, yielding began along four yield lines radiating out from the center of the hole at an angle of approximately 45 degrees. A period of strain hardening then occurred, and the yielding spread in the regions within the initial yield lines, as shown in Figure 2.10.

The specimen shown in Figure 2.10 was fabricated with a A_n/A_g nominally equal to 0.9 (Y/T), significantly less than the 1.2(Y/T) (refer to Equation 1.4). These specimens never yielded significantly on the gross section. The localization of strain in the net section was characterized by gradual necking in both specimen thickness and width. A ductile fracture initiated at the edge of the hole a quickly propagated across the net section, as shown in Figure 2.11. Note that although these specimens failed by net section fracture, they did exhibit at least 2.4% strain and a tensile ductility of about 9.

Figure 2.10 – HPS70W-0.9-L specimen after testing

Figure 2.11 – Fracture Surface of HPS70W-0.9-L Specimen

In the single-hole net-section specimens with A_n/A_g ratios of 1.0 or 1.1 times the Y/T, the initial behavior was essentially the same as the 0.9(Y/T) specimens. The yielding began on lines radiating out from the hole followed by complete yielding of the net section within the initial yield lines. However, at this point, instead of experiencing rapid yield localization and necking on the net section, two horizontal yield lines formed just above and below the furthest reach of the net-section yield zone. The two yield lines then gradually propagated up and down the gage length toward the top and bottom radial transition regions as the yield

strength of the gross-section was developed. Throughout this period of gross-section yielding, the net section continued to experience strain hardening and a resulting increase in load capacity. Following complete yielding of the gross section, necking slowly developed in the net section until specimen failure was experienced by net-section fracture.

Figure 2.12 shows the final state of the test for which the data were shown in Figure 2.9. This failure mode was typical of the 1.0 and 1.1(Y/T) specimens. As evidence of both the increased A_n/A_g ratio and good material ductility, whitewash flaking and yielding can be noted throughout the gage length of the specimen.

Figure 2.12– Final state of HPS70W-1.1-H specimen

Each of the 12 holes experienced the same, four-45° yield line behavior observed for the single-hole specimens. These yield lines connected with those from the adjacent holes to form a yield lattice, as in Figure 2.13. Following yielding along each hole plane, the material contained enough strain hardening capacity to continue to increase its load capacity. However, since the A_n/A_g is only about 0.83 times the Y/T for these specimens, gross section yielding was not expected. Localized strain continued along the yield lattice and initiation of necking on several different hole planes was then observed.

Figure 2.13 –Final state of HPS70W-12h specimen

The final failure was a two-step process. An initial fracture propagated through the ligaments between the hole and the edge of the specimen. The remaining middle ligament then proceeding through full strain hardening, necking and eventual fracture on a shear plane oriented at 45 degrees relative to the loading. A close-up of the fracture surface is shown in Figure 2.14.

Figure 2.14 – Fracture surface of HPS70W-12h specimen

Even though the net section size of the bolted splice specimens was identical to that of the 12-hole specimens (A_n/A_g equal to about 0.83 times the Y/T ratio), the behavior under direct tension was completely different. In the splice specimen, some fraction of the load is transferred from the pull plates into the splice plates at each row of bolts (Kulak and Fisher, 1969). Therefore, the yielding only takes place on the net section at the lead row of bolt holes, since the load is reduced on all the other net sections. Figure 2.15 shows a yield line emanating from the lead row of bolt holes. As it turns out, the deformation is approximately equal from each of the lead rows (top and bottom of specimen), although necking and final fracture eventually occurs on only one of these planes, as shown in Figure 2.16.

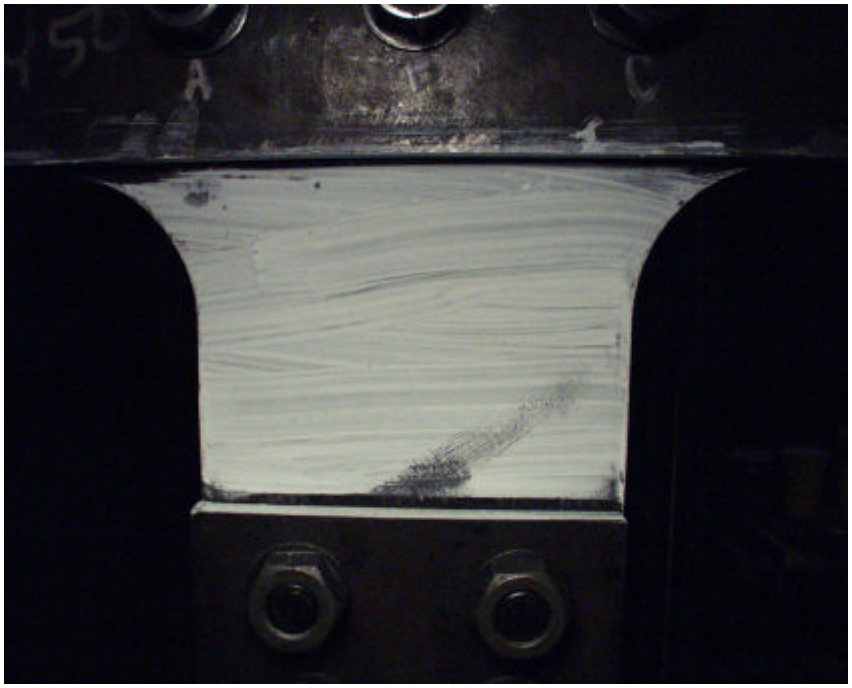

Figure 2.15 – Initial Formation of yield line from critical net section of HPS70W-12hSp

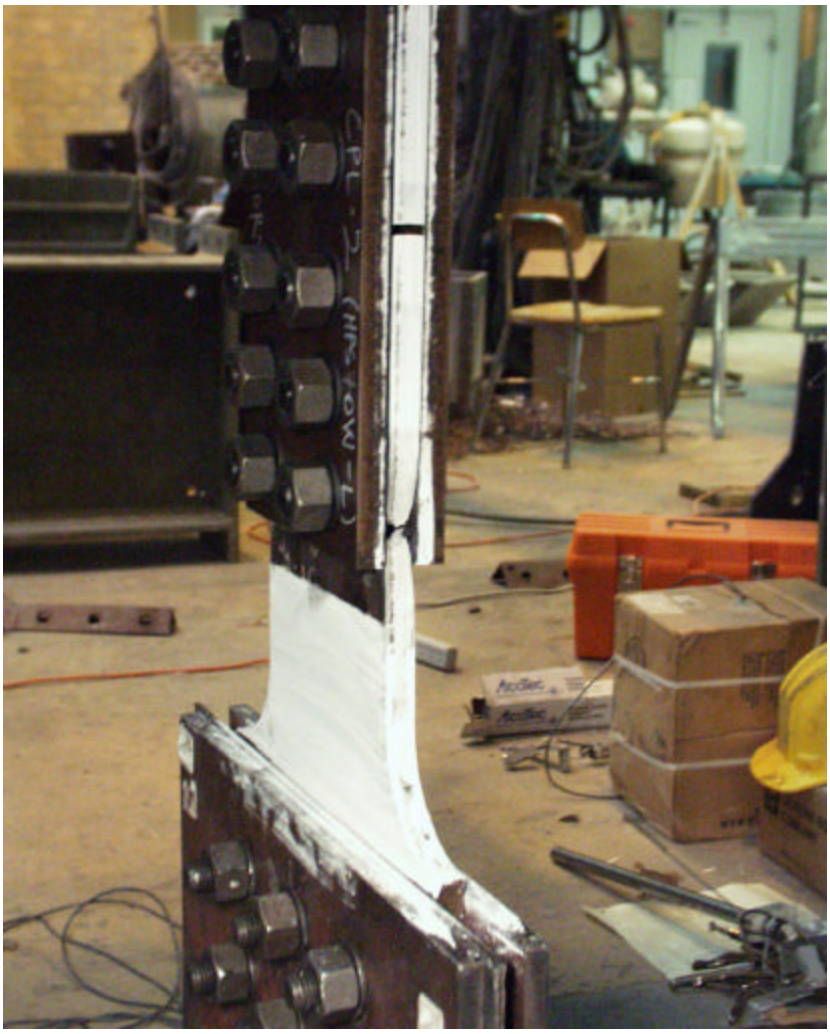

Figure 2.16 – HPS70W-12Sp showing necking on the failure plane

2.2.4 Finite-element modeling of the wide-plate tests

The specimens were modeled using ABAQUS software. Two-dimensional plane-stress elements with reduced integration, element S8R5, were used. This is a thin-shell element with eight nodes and four integration points. Due to symmetry along both the vertical and horizontal plane of all wide-plate specimens, quarter-symmetry models using the appropriate boundary conditions were constructed for each specimen. The longitudinal displacements were imposed on the grip edge and transverse displacements were left unrestrained. A typical specimen model is shown in Figure 2.17. The geometry of each quarter-symmetry model was based upon the net-section and gage-length dimensions of each test specimen.

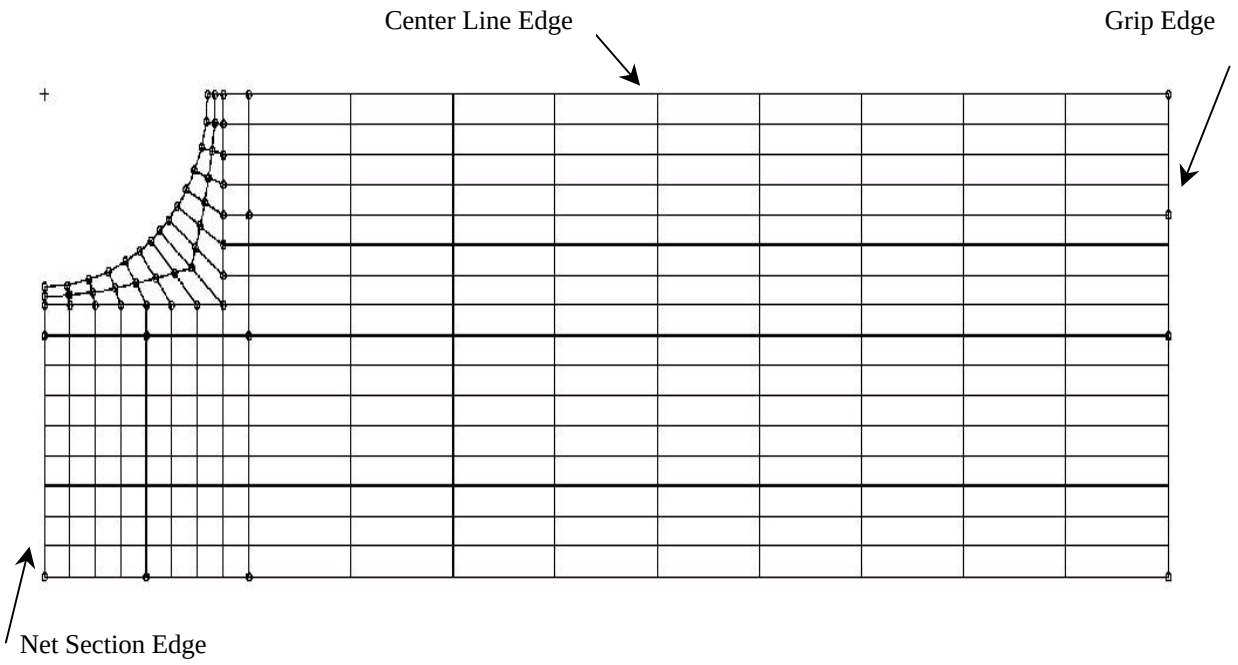

Figure 2.17 – Typical Specimen Finite Element Model

The analyses included the effects of large deformations. The global results such as gross-section stress and elongation from this mesh were compared to a more coarse mesh and were found to have converged sufficiently. Results in the refined area near the hole are obviously going to continue to improve as the mesh is refined. However, the changes in the predicted stresses and strains near the hole as the mesh is further refined have little impact on the global results.

The accuracy of the results, in terms of simulating the experimental results, was dependent on the precise description of the stress-strain curve input to the ABAQUS model. A complete true stress-true strain curve, derived from the monolithic wide-plate tests results, was input in a piecewise linear manner. An analysis was then made with a model of the monolithic specimen. The results were converted back to engineering stress-engineering strain, and were then compared to the actual monolithic test results. The input true-stress vs. true-strain data were adjusted if necessary until the results of the analysis of the monolithic specimens were in good agreement with the results from the experiment.

This material stress-strain curve was then used to predict the results of the experiments with various hole sizes. It was verified that in the elastic range the stress predicted at the edge of the hole was equal to three times the nominal gross section stress. The gradient of the stresses across the net section in the elastic range also compared almost exactly to the analytical stress gradient curve from a solution method presented in Timoshenko and MacCullough (1949).

Predicting large-deformation necking behavior of plates in tension can be very difficult and in the end is sensitive to the type of imperfection used to trigger the localizations. Therefore, it was not attempted in these finite-element analyses to predict the actual onset of

failure. Instead, the model would continue to predict continued deformation without localization and failure. Nevertheless, it is useful to be able to predict the load vs. elongation curve up to the failure point. Therefore, the finite-element results (net-section and gross-section strength) are recorded from the finite-element analyses at the elongation corresponding to the elongation at failure in the experiments.

Despite the numerous possible sources of variability, the deviations between the experimental net-section and gross-section strength data and the finite element data were quite small. For all three grades of steel, the finite element models slightly over-predicted the measured ultimate capacities of the specimen net sections. The models also consistently provided predictions of maximum developed gross-section stresses that were below the experimentally measured quantities.

The ABAQUS analyses were very effective in confirming these experimental test results. The finite element models also provided the study with results for hypothetical specimens outside the range of net-section properties experimentally examined.

2.2.5 Analyses of the wide-pate test results

Analysis of the test results and finite-element results indicated that the load and elongation of the various materials and specimens could be correlated if they were plotted in terms of the ratio of A_n/A_g to the measured Y/T of the monolithic wide-plate specimens. Another way to look at this parameter is as the nominal strength of the net section to the nominal strength of the gross section (without resistance factors). Figure 2.18 shows the maximum gross-section stress for the variety of HPS-70W specimens. In Figure 2.18, the A_n was based on the actual net area, rather than the design approach where the hole size would be increased by 1/16 inch in order to compute A_n.

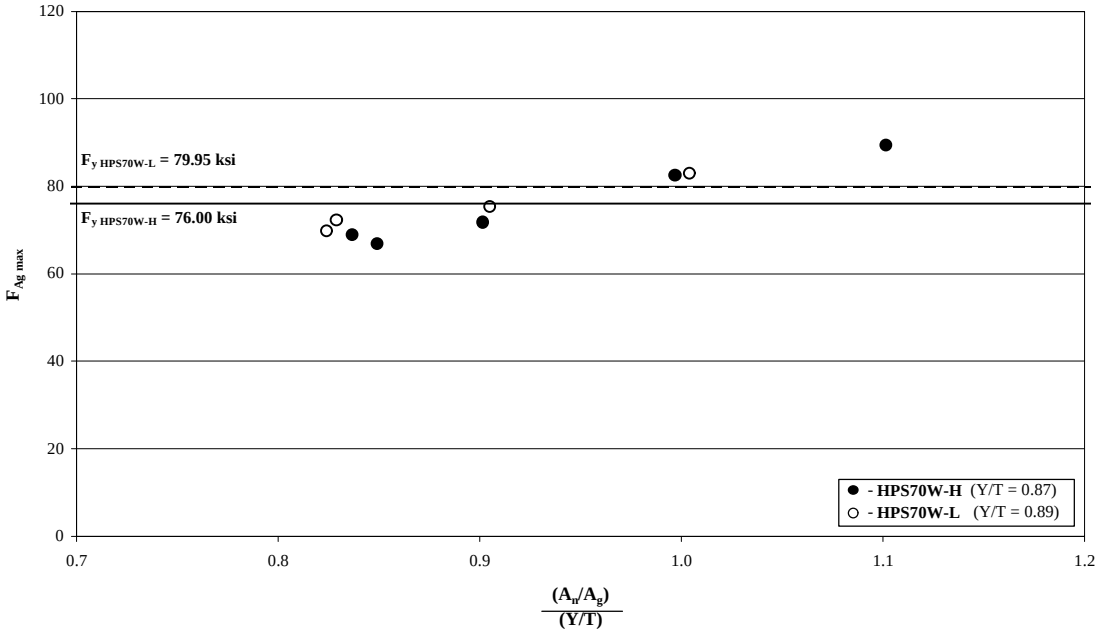

Figure 2.18 - Experimental gross-section stress for HPS70W specimens

The 12-hole specimens and the spliced specimens are shown to the left at a $(A_n/A_g)/(Y/T)$ ratio between 0.8 and 0.9. The monolithic specimen results are shown at the right end of the plot, at a $(A_n/A_g)/(Y/T)$ ratio equal to the inverse of the Y/T (since A_n/A_g is equal to one). The yield strength of both HPS70W samples, as taken from the apparent yield point of the monolithic specimens, is indicated on Figure 2.18. A nearly linear upward trend is observed in the data, which reaches the yield stress on the gross section at a $(A_n/A_g)/(Y/T)$ ratio slightly less than 1.0.

Figure 2.19 includes the results from the A709 Grade 50 and HPS100W specimen tests and from finite-element simulations. To compare the results of all three materials in an equivalent manner, the gross section stresses in Figure 2.19 are normalized by the yield strength measured with the monolithic specimens. The data were also plotted in terms of the A_n based on the hole size increased by 1/16 inch. This change has no effect on the gross-section area, and therefore produces no change in the maximum gross-section stresses developed. Thus, no vertical change in the data points of Figure 2.19 takes place. But, this hole allowance does decrease the net-section area, having the result of shifting all the data points in Figure 2.19 to the left slightly, as shown in Figure 2.20.

The second quantity examined is the ultimate capacity on the net section of the specimen. Figure 2.21 shows the net section stress, which is the peak load divided by the original net-section area, normalized by the ultimate strength of the monolithic specimen, as a function of the $(A_n/A_g)/(Y/T)$ ratio. The most impressive characteristic of Figure 2.21 is that the ultimate strength is reached on the net section even for net-section ratios as low as 0.9 and 0.8.

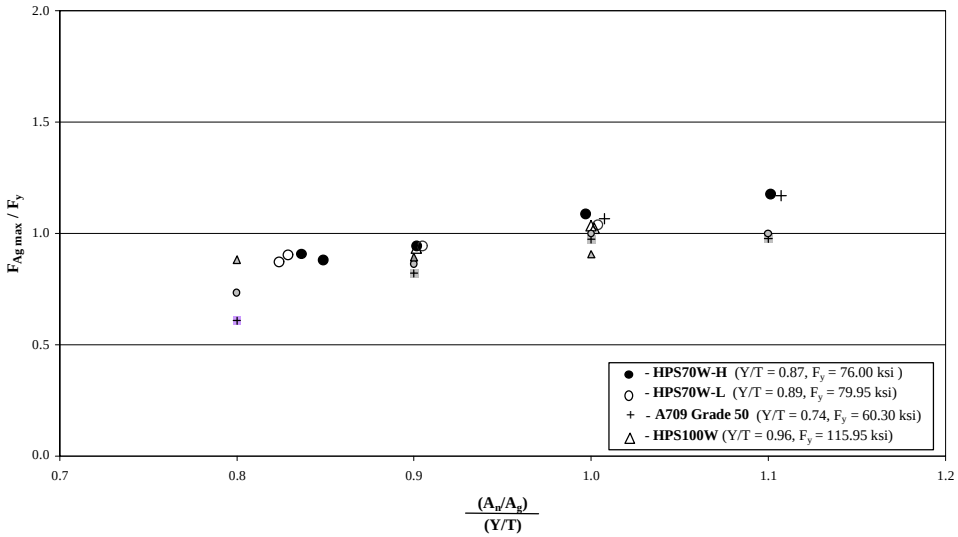

(Finite-element results are shaded symbols.)

Figure 2.19 - Experimental and finite-element gross-section stress for all grades of steel

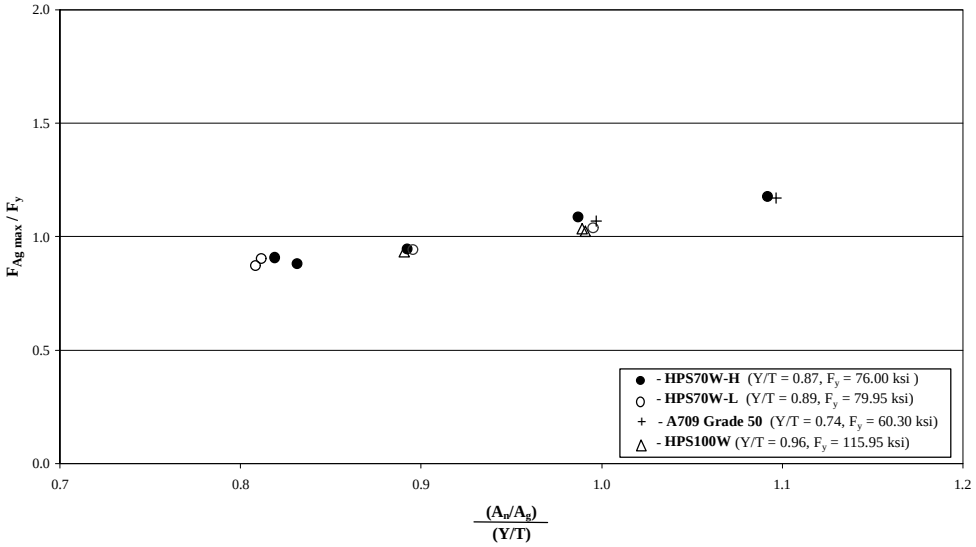

Figure 2.20 - Experimental gross-section stress for all grades of steel where A_n includes the 1/16 inch allowance on the hole size

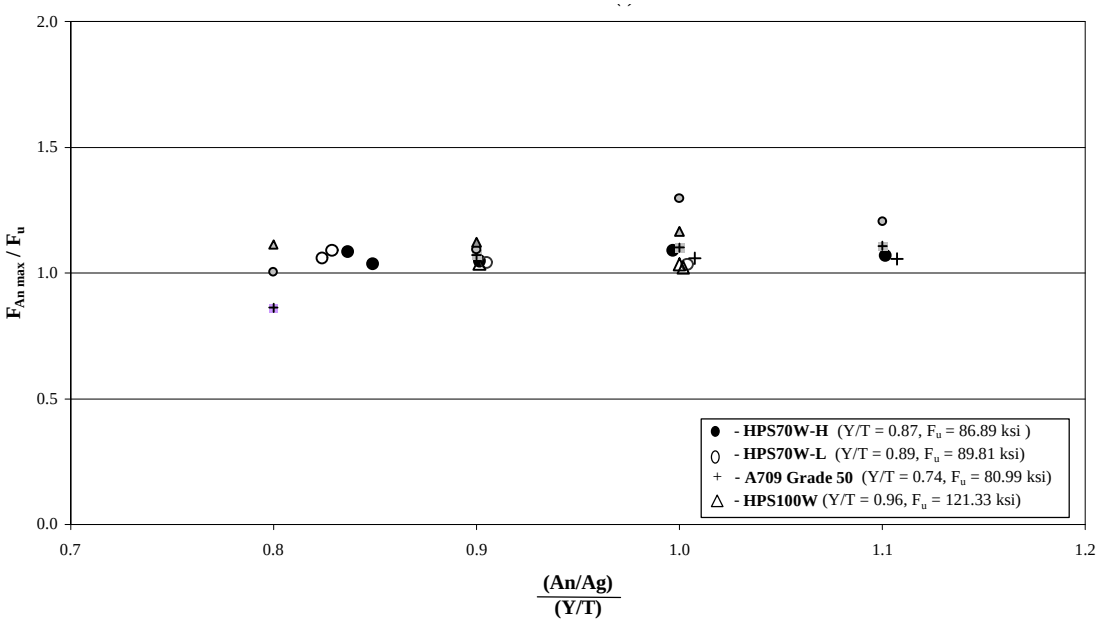

(Finite-element results are shaded symbols.)

Figure 2.21 - Experimental and finite-element net-section stress for all grades of steel

Figure 2.22 shows the same data from the experiments re-plotted in terms of the A_n including th 1/16 allowance on hole size. In addition to shifting the data to a slightly lower $(A_n/A_g)/(Y/T)$ ratio, the allowance also has the effect of increasing the apparent net-section stress slightly. These effects are both conservative and therefore the actual net section data can be used conservatively.

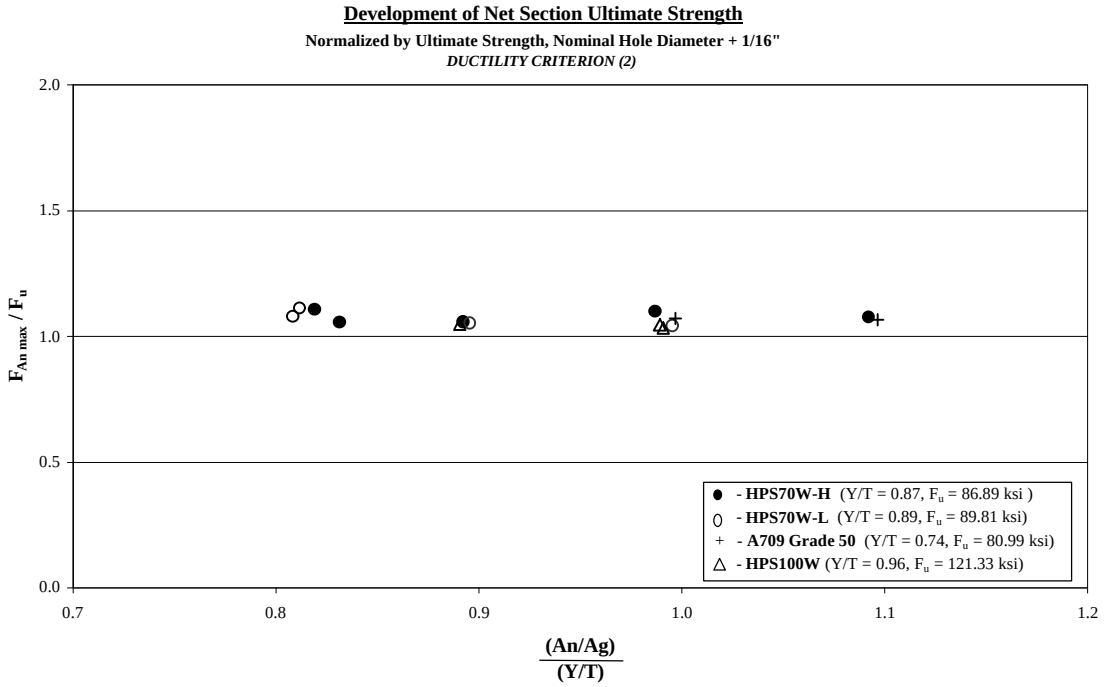

Figure 2.22 - Experimental net-section stress for all grades of steel where A_n includes the 1/16 inch allowance on the hole size

The most important criterion that was measured in these tests is the elongation and ductility. The maximum gage length elongation with respect to $(A_n/A_g)/(Y/T)$ ratio is shown in Figure 2.23 for all grades of net-section specimens. A general upward trend is observed. Elongation on the order of 3% was reached at an $(A_n/A_g)/(Y/T)$ ratio of 1.0. This is more than enough strain to satisfy the demand in ordinary composite flexural members, as in the

experiments conducted at University of Nebraska – Lincoln (Mans 2002). If greater elongations were required, say for the demand of about 6% in the girder flexural test described in the next section, then the $(A_n/A_g)/(Y/T)$ ratio should be equal to or greater than 1.1.

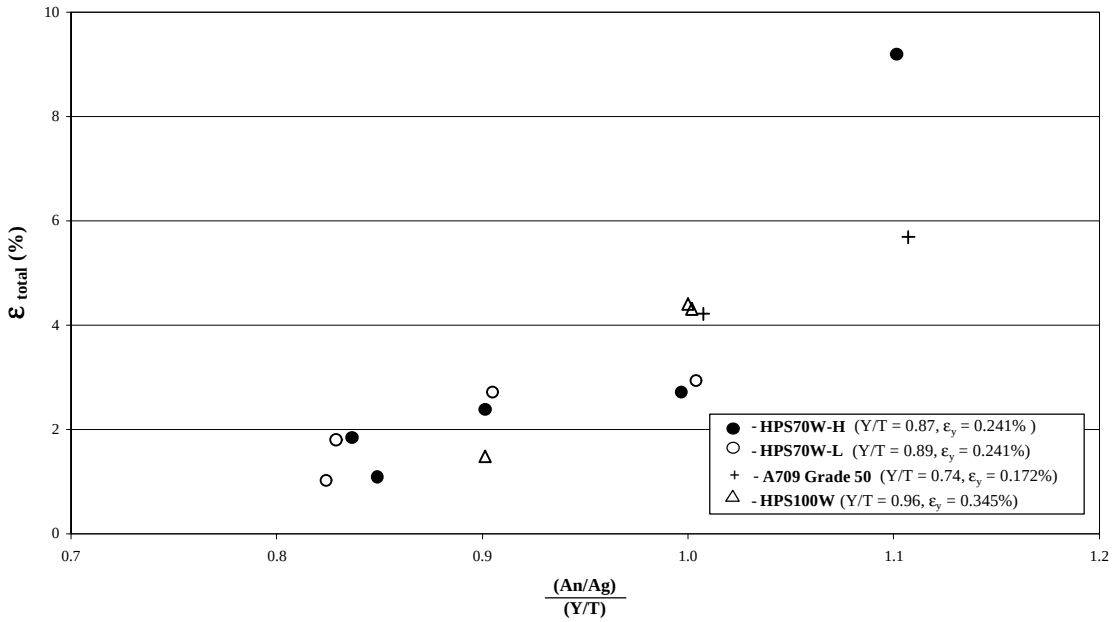

Figure 2.23 - Maximum gage-length elongation for all steel grades

Alternately, the elongation data could be normalized by the yield strain, as in Figure 2.24. This is the way the data are normalized in the tension ductility calculation in Equation 2-1. However, there is more apparent scatter between different types of materials when elongation is normalized by the yield strain. This normalization favors the grade 50 steel (since the elongation is dividing by smaller denominator) and penalized the HPS100W specimens (since it is dividing by larger denominator).

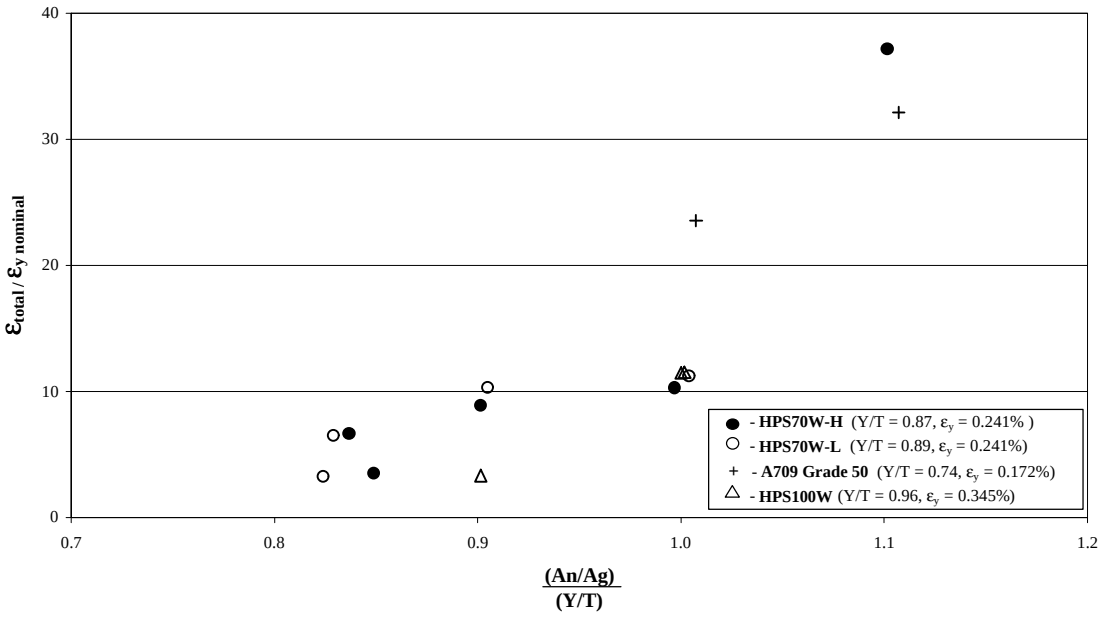

Figure 2.24 - Maximum gage-length elongation normalized by yield strain

The elongation results were not plotted in terms of the A_n that includes the 1/16 inch allowance on the hole size. However, based on the previous comparisons, it is known that this would not affect the elongations and would only cause a slight shift to a lower vales of $(A_n/A_g)/(Y/T)$ ratio.

In summary, these wide-plate test data show that the net section behavior for a range of structural steels can be explained entirely by the $(A_n/A_g)/(Y/T)$ ratio. The results show that as long as the $(A_n/A_g)/(Y/T)$ ratio is 1.0 or greater, gross section yielding can be achieved as well as adequate ductility (i.e elongation greater than 3% or tensile ductility greater than 10). Ultimate strength is achieved on the net section regardless of the $(A_n/A_g)/(Y/T)$ ratio, even for $(A_n/A_g)/(Y/T)$ ratios as low as 0.8.

In the range tested, the finite element data shows good agreement with the experimental results and among the various grades of steel.

The results show very little variability between each grade of steel. The lack of variation between materials provides evidence to broaden the conclusions to all types of structural steel.

2.3 Girder test

As discussed in Section 1.2, one girder with HPS70W web and tension flange was fabricated and tested to failure. This girder was tested to investigate the potential for tension flange rupture in a girder and to relate tension panel ductility to girder ductility.

2.3.1 Girder test specimen

The test specimen was shown in Figure 1.1. The specimen design was constrained by the 660 kip capacity of the test machine. The HPS-70W tension flange was the same cross section as the wide-plate tension test specimens; 8-inches wide and 0.75-inches thick. Since it was impractical to build a composite section in the lab, a very large Grade 50 compression flange 8 inches wide and 3.5 inches thick was used to shift the plastic neutral axis up to the top flange and to eliminate the possibility of flange local buckling. The 26-inch deep web (giving an overall depth of 30.25 inches) was made from 0.75-inch thick HPS-70W plate so that shear buckling could not occur and no stiffeners were required. Bearing stiffeners on both sides of the web were placed at midpsan and at the supports.

2.3.2 Girder test procedure

The girder was supported on roller supports with a span of 20 feet. McDermott's tests that resulted in tensile flange rupture were loaded in three-point bending, i.e. there was a moment gradient at the location of the plastic hinge. Therefore in order to test the worst-case scenario, this test was also conducted in three-point bending. Lateral braces were provided five feet from the supports, and the compression flange was also braced by the test machine at midspan, giving an unbraced length of 60 inches. The weak axis bending stiffness of the compression flange is such that lateral-torsional buckling (LTB) should be suppressed for an unbraced length of 92 inches (according to AASHTO LRFD design criteria).

High-elongation strain gauges were place along the tension flange and web. As seen in Figure 2.25, five strain gauges were placed along the vertical line 15 inches from the centerline to verify the linearity of the strain gradient and the neutral axis location. Six strain gauges were placed along the tension flange from the center to the south support to measure the strains at different locations along the length. Seven LVDT's were place at along the length of the girder to measure deflections. In addition, LVDT's were placed at the south end of the girder to measure the end rotation.

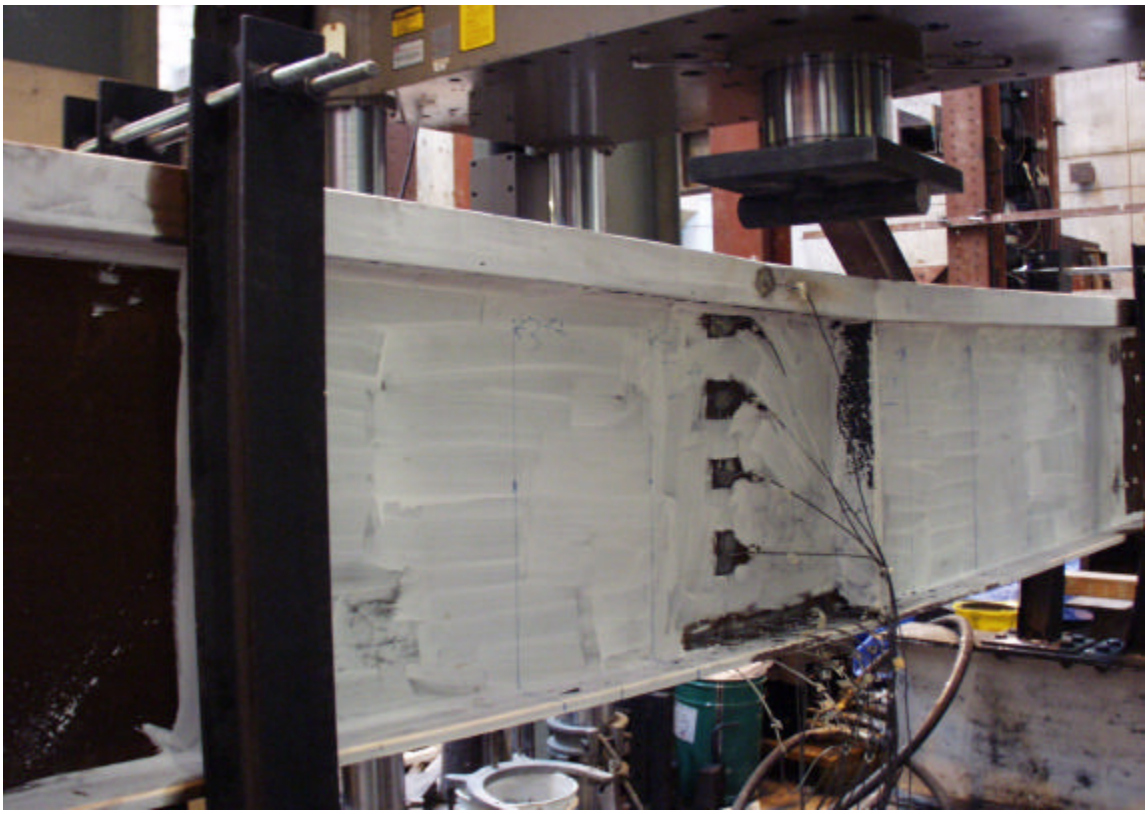

Figure 2.25 –View of girder specimen after testing showing permanent plastic rotation as well as web strain gage locations

The loading was displacement controlled at a stroke rate of 0.0024 in/s, which corresponded to a strain rate in the elastic range of 10^{-5} sec^{-1} in the tension flange. Several elastic cycles up to 130 kips were applied before the final test was performed.

2.3.3 Girder test results

It was expected that the girder would start to yield at 360 kips. Analysis of the strain gauge data showed that the initial yielding occurred at a load of 380 kips. The load to develop the plastic moment, 2950 ft-kips, was estimated to be 590 kips. The ultimate load experienced by the girder was 652 kips, creating a moment at the center of the girder equal to 3260 ft-kips.

The web experienced nearly complete plastification. This can be seen from the web strain gauge data shown in Figure 2.26, which shows the strain distribution in the web at 2850 ft-kips, just before the plastic moment.

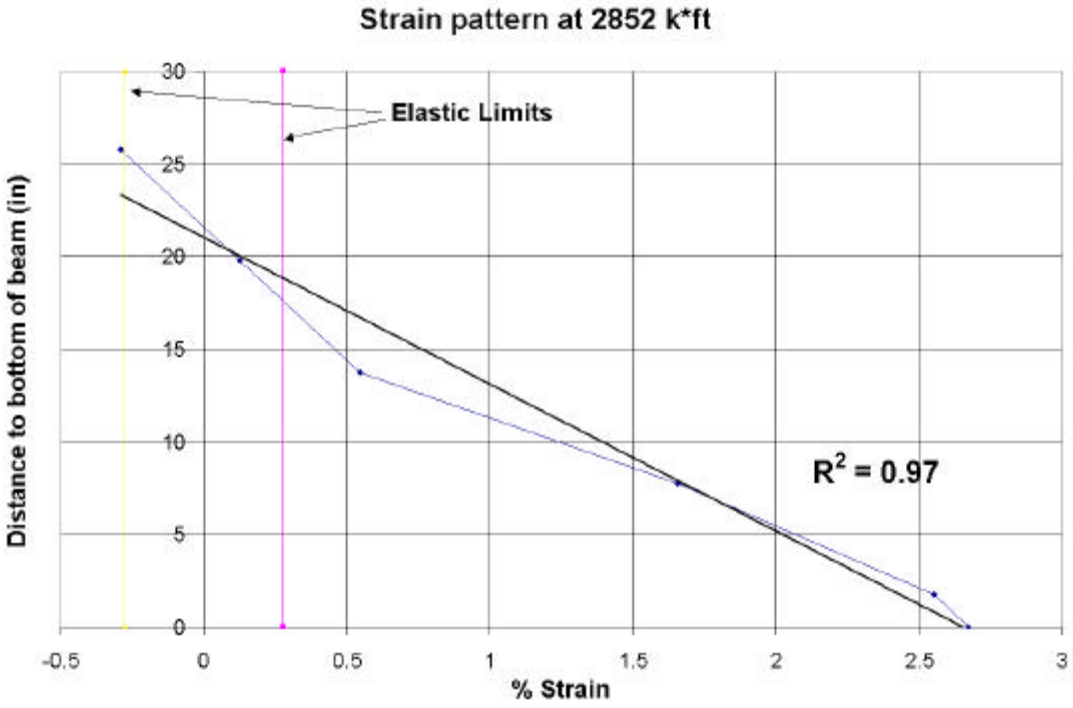

Figure 2.26 –Distribution of longitudinal strain on cross section near beam centerline at 97% of plastic moment

Figure 2.27 shows the deflected shape as measured with the LVDT's near the end of the test. Rotation was measured at the south end support with LVDT's and was also estimated from the midpoint deflection divided by the half span length (this will be referred to as the Δ/L approximation). The end rotation is always slightly greater than the rotation from the Δ/L approximation, as shown more clearly in the blown-up view of the deflected shape near the end of the girder in Figure 2.28.

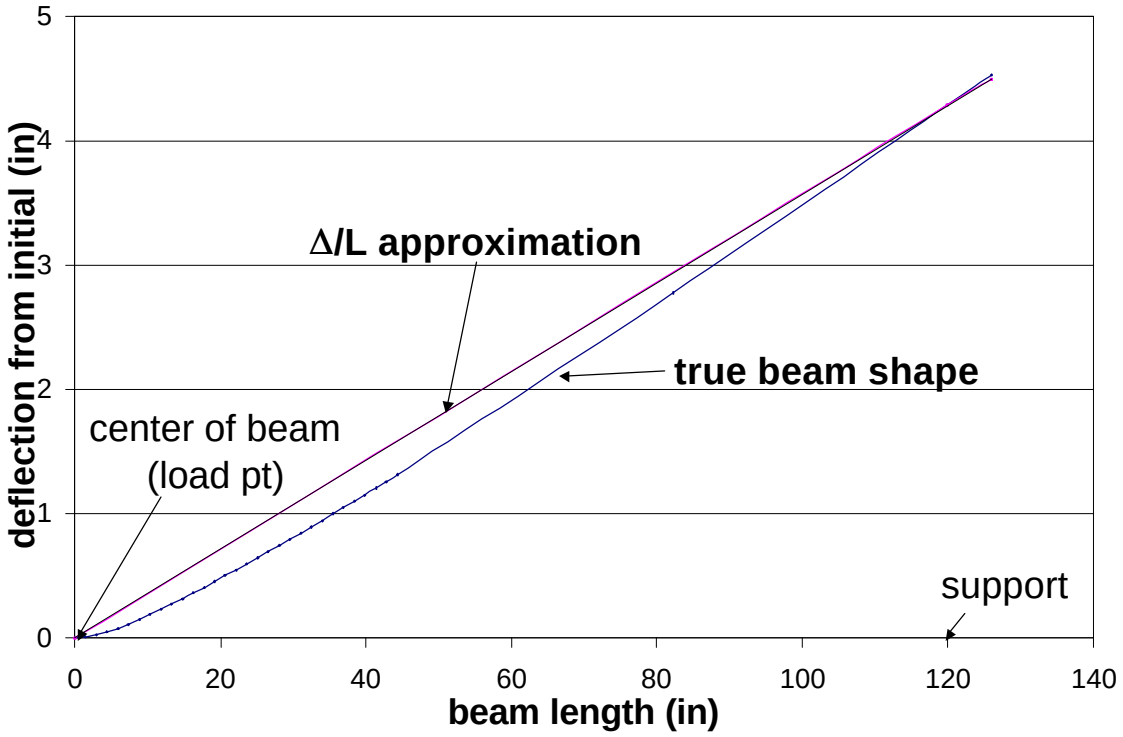

Figure 2.27 – Measured displaced shape of the beam near the end of the test compared to the secant Δ/L approximation for a rigid-perfectly-plastic beam

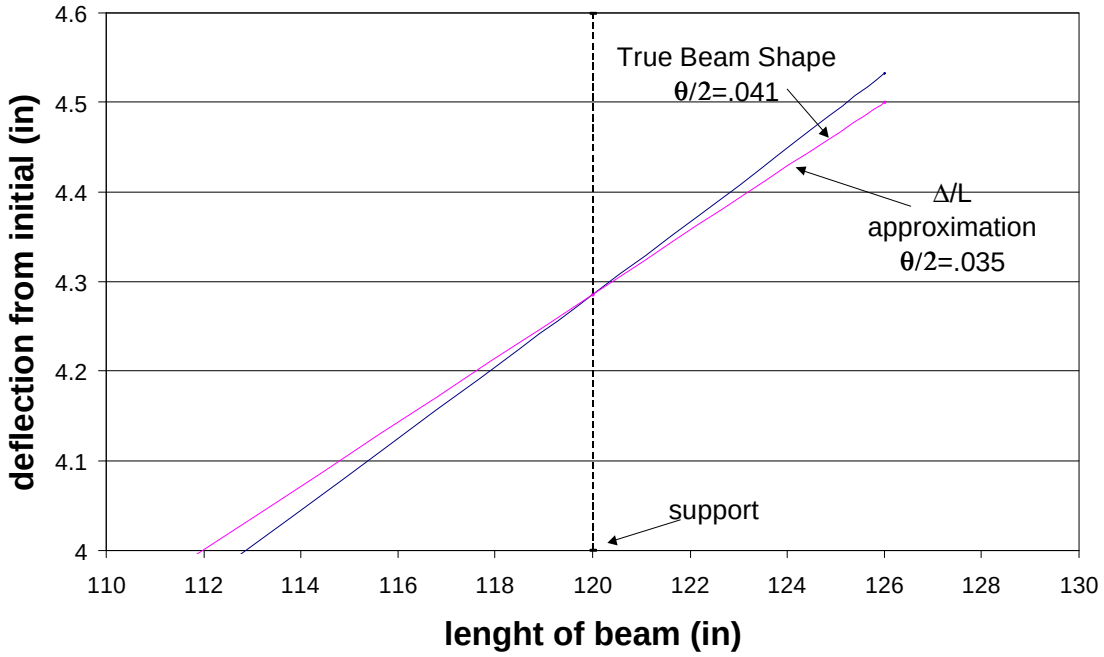

Figure 2.28 – Close-up view of the measured displaced shape near the support showing difference between methods of measuring rotation

The moment rotation curve was shown in Figure 1.3. The maximum moment was attained when the rotation got to be about 8.5%. The moment was approximately steady as the rotation increased to about 11.4%, at which point there was a sudden lateral-torsional buckling failure. A photograph of the tension flange after testing is shown in Figure 2.29. The tension flange did not begin necking or premature rupture. The maximum strain measured on the tension flange was 6.5% just before failure.

Figure 2.29 – Photograph of the tension flange after testing

2.3.3 Analysis of the girder test

A simple cross-section analysis model was developed to predict the moment vs. rotation behavior of hybrid unsymmetrical cross sections. The numerical solution is based on flexure theory using the stress vs. strain data from the HPS70W coupon test. The coupon stress-strain curve was divided into the traditional regions including elastic, yield plateau, and strain hardening. The elastic region was modeled assuming a modulus of elasticity of 29,000 ksi. The elastic curvature ϕ was determined according to M/EI. The curvature was integrated along the length of the girder to find the rotation and associated deflections.

When the yield point was reached on the tension flange, the remaining incremental behavior was found with an iterative elastic-plastic model. The yield plateau was perfectly plastic with strength equal to the measured yield strength (80 ksi for the web and tension member and 61 ksi for the compression flange). The neutral axis is based on the stress distribution and the stress is dependent on the strain. However, the neutral axis must be known before the strain can be predicted, since all that is known from the curvature is the strain gradient.

A spreadsheet was set up with these relations. An initial guess of the neutral axis was made, and then the apparent location of the neutral axis was determined from equilibrium on the cross section. The stress in each section is computed from the strain. It is then determined what stress distribution will be used. There are five possible modes, depending on the magnitudes of the strains.

The first mode, shown in Figure 2.30a, is the common flexural behavior where the tension flange, compression flange and web all remain in the elastic range. The second mode is when the tension flange has yielded, while the compression region is still unyielded, as shown in Figure 2.30b. The third mode is characterized by the start of yielding on the outer most fibers of the compression flange, as shown in Figure 2.30c. At this point, the neutral axis is moving up the girder toward the top flange.

The fourth mode, Figure 2.30d, is characterized by the yielding of the compression section of the web and the start of strain hardening in the tension flange. At this point the neutral axis starts to shift back toward the tension flange. Finally, the fifth mode is the characterized by the strain hardening in the compression flange, as shown in Figure 2.30e. This fifth mode was sufficient to characterize the maximum moments and curvatures.

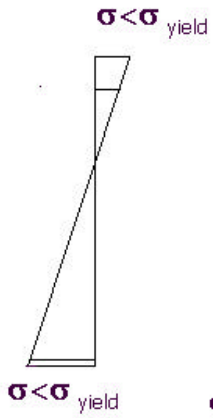

a) Assumed stress distribution in the elastic range (first mode)

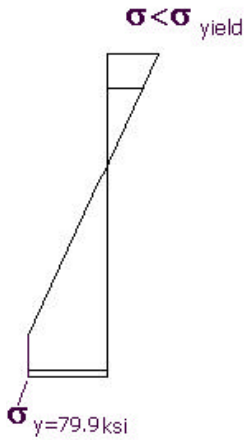

b) Assumed elastic-plastic stress distribution after tension flange yielding (second mode)

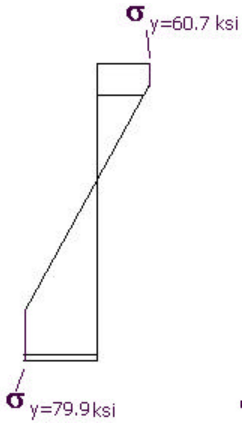

c) Assumed elastic-plastic stress distribution after compression flange yielding (third mode)

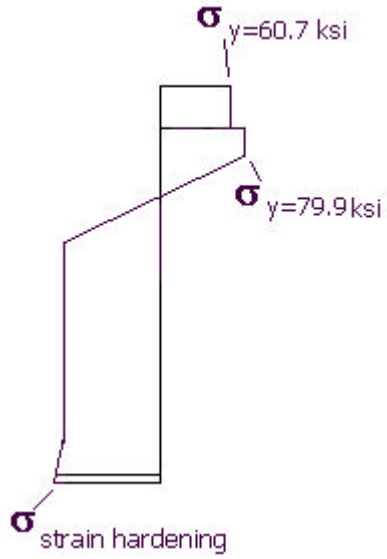

d) Assumed elastic-plastic stress distribution after web yielding in compression and tension flange strain hardening (fourth mode)

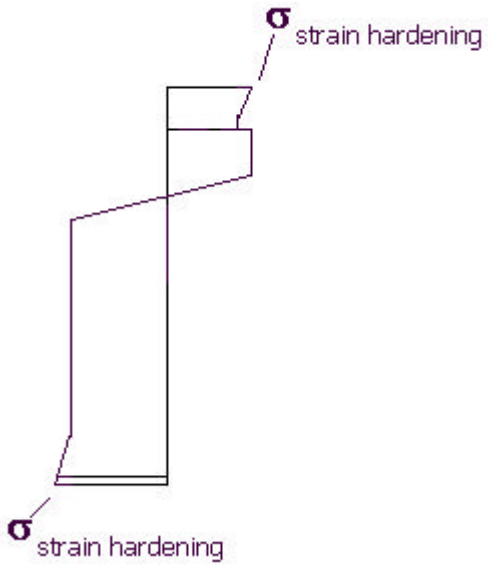

e) Assumed elastic-plastic stress distribution after strain hardening in compression flange (fifth mode)

Figure 2.30 – Cross-section analysis of girder

The result from these calculations was an array of moment-curvature pairs. The moment diagram is deterministic, so a curvature can be found for each discrete point on the moment diagram. The yield moment was calculated and used to determine the length on the girder that was inelastic, as shown in Figure 2.31.

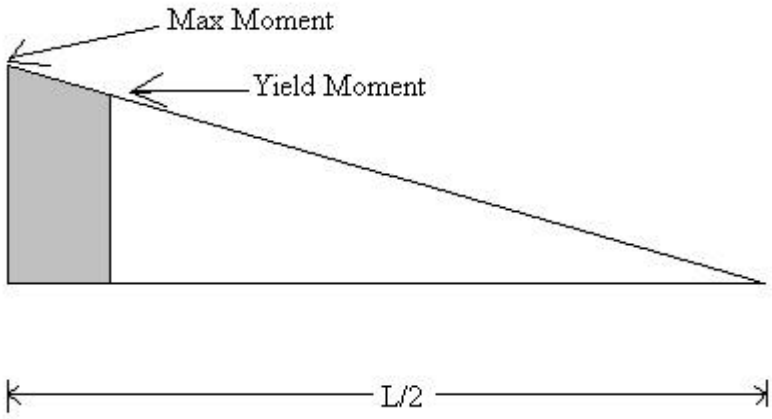

Figure 2.31 – Bending moment diagram for the half beam length

The inelastic part of the beam length was then divided into segments 1.5 inches in length and an average curvature was assigned to each segment, as shown in Figure 2.32. This curvature diagram was integrated to get rotations and displacements. This analysis can predict the moment-rotation behavior up to failure but it does not predict when the failure will occur. Figure 2.33 shows a comparison of the predicted moment vs. rotation curve to the measured moment vs. rotation curve, which was originally shown in Figure 1.3. The tension flange strain from this analysis was also reasonably consistent with the measured strain in the tension flange.

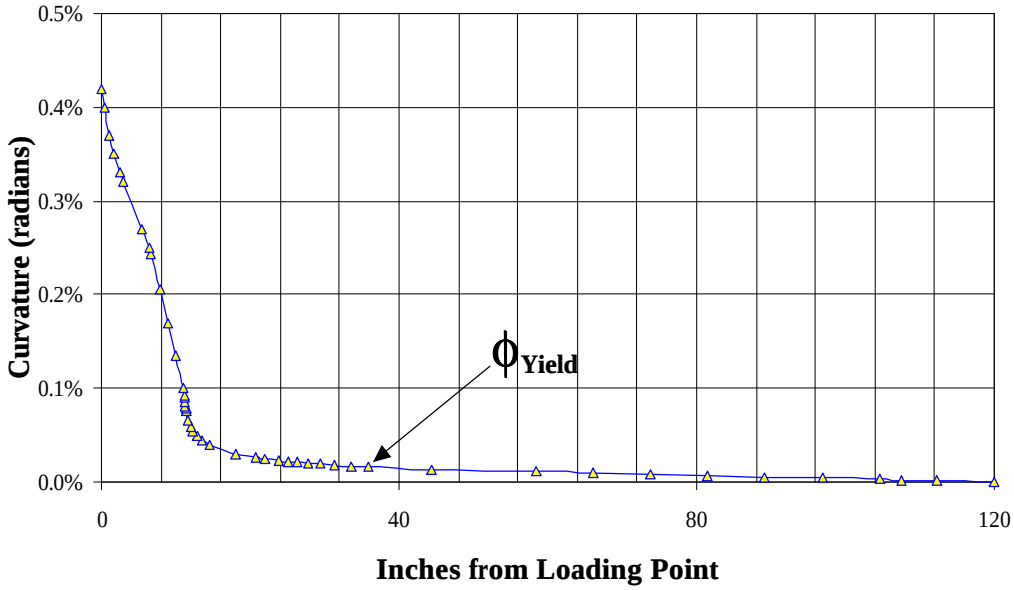

Figure 2.32 – Curvature diagram for the half beam length

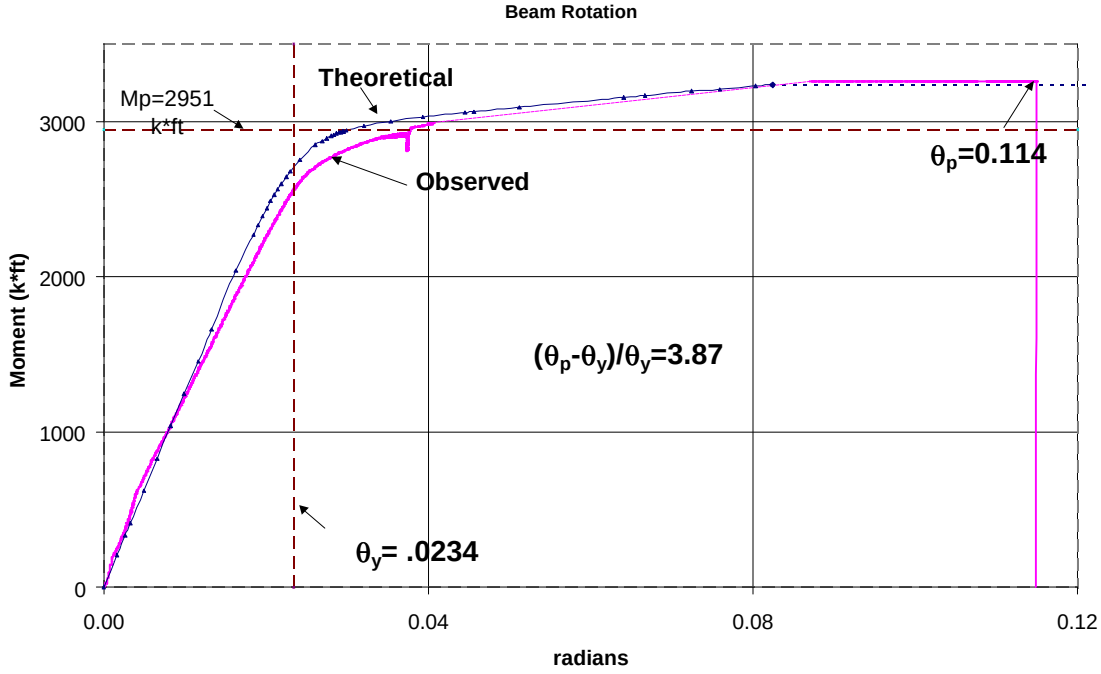

Figure 2.33 – Comparison of predicted and measured moment-rotation curves

3.0 Statistical analysis of Y/T data

The wide-plate test results presented in Section 2.2 suggest that adequate ductility (i.e elongation greater than 3% or tensile ductility greater than 10) is obtained as long as the $(A_n/A_g)/(Y/T)$ ratio is 1.0 or greater. In other words, if the Y/T is known, γ in Equation 1.4 need not exceed 1.0 (or equivalently that the number 0.84 in Equation 1.5 or 1.7 need not be less than 1.0). However, as discussed in Section 1.4, the Y/T is not known exactly, only the ratio of the minimum specified values F_u/F_y. As was shown in Table 1.1, each type of steel has a unique distribution of possible Y/T values and a unique relationship between the mean Y/T and the ratio of the specified values F_u/F_y.

Statistical data on the variation of Y/T were studied to determine adequate margins of safety to use in the design equations. An upper bound or safe Y/T value was derived for the grades of steel in Table 1.1 including HPS70W steel. The safe Y/T value was compared to the F_y/F_u ratio to compute an appropriate γ factor for proposed improved design equations as an alternative to the ratio of the ϕ factors.

Data for A36, A572, A588, and A514 steel plate was obtained from a study by Brockenbrough (1995), while data for A992 shapes were obtained from a study by Dexter et al (2001). Tensile test data for 2459 heats of HPS70W were obtained from two mills of one producer.

Figure 3.1 shows the Y/T plotted as a function of thickness It can be seen that the high Y/T values are typically found in thcknesses less than 2 inches. In fact, only one heat of the almost 300 heats greater than 2 inches thick had Y/T greater than 0.91. The data were analyzed separately for thickness up to and including 1 inch, from 1 to 2 inches, and greater than 2 inches. There was not a significant difference between the Y/T statistics for the data

up and including 1 inch and the data from 1 to 2 inches. Therefore it was decided to group all the data from both mills up to and including 2.0 inches thick into one database for statistical analysis. If the design rules derived from these data are applied to thicker plates, the result will be conservative since the thicker plates tend to have lower Y/T.

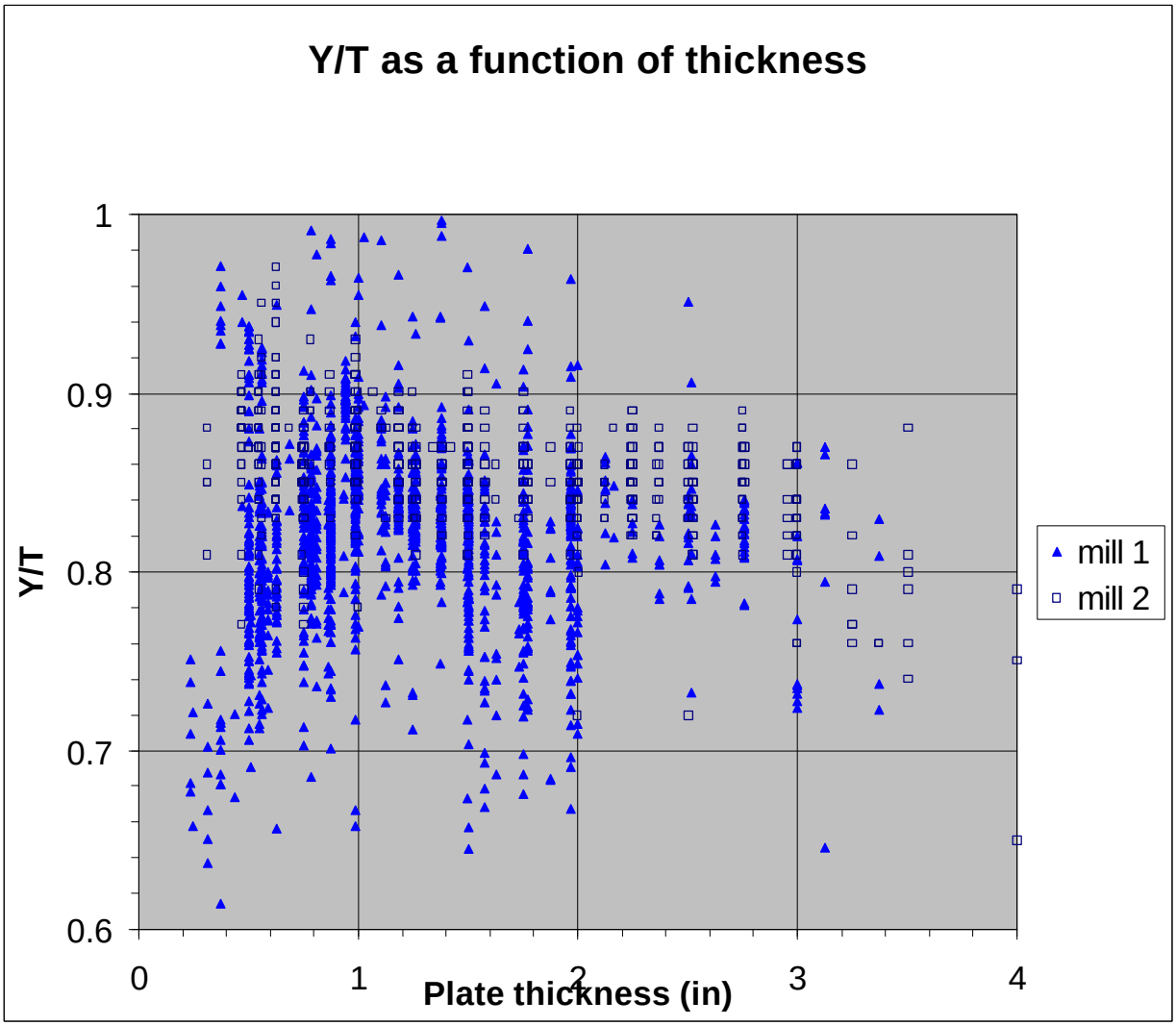

Figure 3.1: Y/T data for HPS70W

Figure 3.2 shows a histogram of the Y/T data for the 2164 heats with thickness less than 2.0 inches At the top of each bar in the histogram is the percent occurrence, and the cumulative probability is shown as a solid line. It can be seen that the assumption of a normal distribution is reasonable, even though it is clear that the tails of the distribution are limited. The box in Figure 3.2 gives a summary of the statistics of the distribution, indicating the mean is 0.835 and the COV is 5.99%.

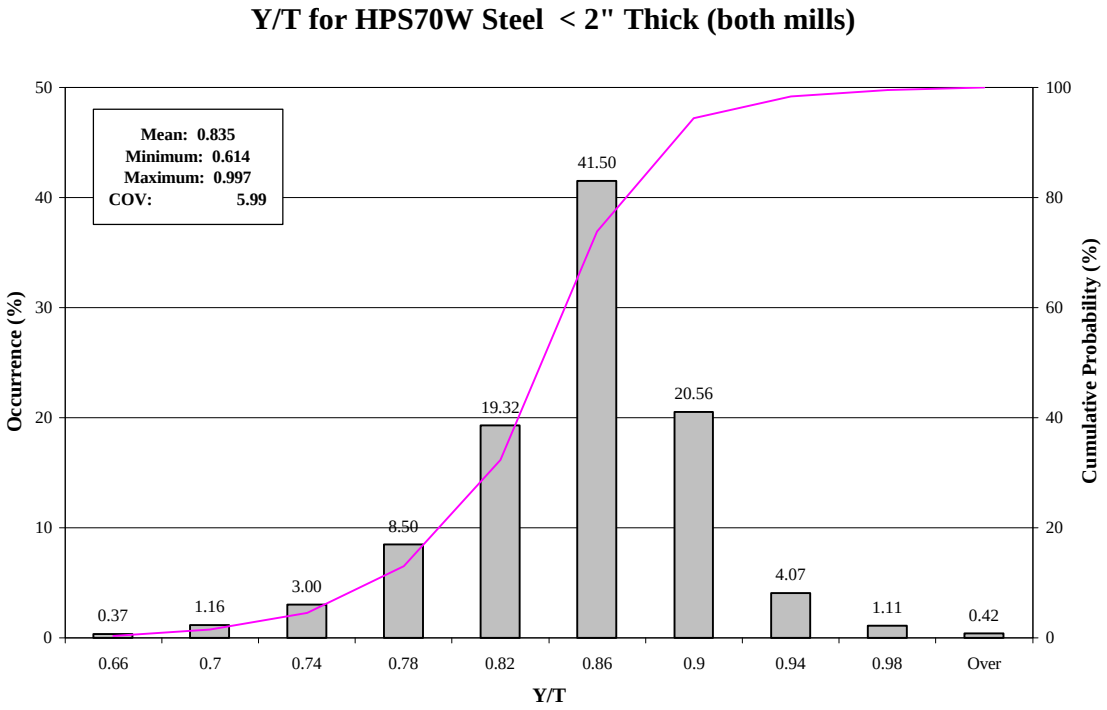

Figure 3.2: Histogram of Y/T data for HPS70W

As discussed in Section 2.1, the two heats of HPS70W had Y/T of 0.87 and 0.89, i.e. about one standard deviation greater than the mean. Thus, the heats of HPS70W that were tested represent the high range of Y/T for this steel.

Given an appropriate reliability index β, an upper-bound or safe Y/T value may be selected for HPS70W steel or any other steel. (Note, this β is not the same as the β in Equation 1.6.) The safe Y/T value can be compared to the ratio of the minimum specified values to see if there is a need for a γ factor greater than 1.0 in the design equation. Note that this process is the opposite of typical applications of reliability such as yield strength, where a lower-bound yield strength F_y is used in design. In the case of the Y/T ratio, a greater Y/T is more detrimental, so an upper-bound Y/T is used in design.

The AISC reliability equation, modified for this problem, is:

$$\gamma R_{n\,Y/T} = R_{m\,Y/T} \times e^{0.55 \beta V_r} \qquad \text{Eq. 3-1}$$

$\gamma R_{n\,Y/T} = \gamma\ (F_Y/F_u)$

$R_{m\,Y/T}$ = mean value of Y/T

β = reliability index

V_r = COV of the Y/T distribution

It is not clear what the appropriate level of reliability should be in order to obtain a safe value of Y/T to use in design equations. If the Y/T turns out to be greater than the safe value, the consequences are only that a net section failure may occur rather than a gross section failure, i.e. only the ductility is reduced but the strength is not reduced. Therefore it seems reasonable that the reliability index β could be less than is used for strength limit states. A β of 2.6 was used for strength limit states in members in the AISC calibration while 3.5 was

used in the AASHTO LRFD specifications. A β of 4.0 is used for connections. For comparison, the results in Table 3.1 were computed for β equal to 2, 2.6, and 3.5.

Table 3.1: Parameters of Y/T distribution and safe Y/T ratios for various levels of reliability

Steel	F_y/F_u	mean Y/T	COV	β=2.0		β=2.6		β=3.5	
				safe Y/T	γ	safe Y/T	γ	safe Y/T	γ
A36 t>0.75"	0.62	0.61	0.080	0.67	1.07	0.68	1.10	0.71	1.15
A572 50 t >0.5"	0.77	0.72	0.052	0.76	0.99	0.77	1.00	0.80	1.03
A588 50 t <2"	0.77	0.74	0.066	0.80	1.03	0.81	1.06	0.84	1.09
A992 shapes	0.77	0.76	0.04	0.79	1.03	0.81	1.05	0.82	1.07
A514 t<2.5"	0.87	0.94	0.017	0.95	1.10	0.96	1.11	0.97	1.12
HPS70W	0.82	0.84	0.060	0.89	1.08	0.91	1.10	0.93	1.14

From the results in Table 3.1, it is clear that the γ factor of 1.2 resulting from taking the ratio of the ϕ factors in the present AISC and AASHTO design equations is far too conservative for any steel. The γ factor for the grade 50 steels is less than 1.1 regardless of the β. In fact, when β is only 2, the worst-case γ factor is 1.03 for any of the grade 50 steels. Considering the typical level of accuracy of engineering calculations, this γ factor of 1.03 seems close enough to 1.0 to warrant keeping the design equations simplified.

Using a γ factor of 1.0 would not be conservative for A36 steel, according to the computed γ factors in Table 3.1. However, there is little concern for the ductility of A36 steel and the area of the holes in the net sections that are allowed are more than is usually required due to low ratio of F_y/F_u (0.62). Therefore, it seems reasonable to keep a γ factor is 1.0 for all steel with MSYS of 50 or less.

Even though the statistics of A514 and HPS70W are quite different, by coincidence the γ factors associated with each level of reliability are approximately the same. Therefore, it seems reasonable to define a γ factor of 1.1 for all steel with a MSYS greater than 50 ksi. A higher level of reliability ($\beta = 2.6$) is provided for the safe Y/T value for high-strength steels than is provided for Grade 50 steels and this is appropriate given the greater concern for the ductility of high-strength steels. If other high-strength steels are used, a survey of their Y/T should be conducted and the γ factors calculated especially for that steel using Equation 3.1 with β of at least 2.6. Also, the distributions of Y/T values should be reevaluated for all steels every decade to see if they are changing due to changes in raw materials and production.

These reliability analyses anticipate that the Y/T for these steels may occasionally be greater than the "safe" Y/T calculated above. This is analogous to the accepted fact that the yield strength may occasionally be below the MSYS. In both cases, the possibility of the material property being outside the specified range is included in the calculation of the probability of failure, and that probability is deemed to be acceptably small. Therefore, it is not recommended that specification limits on the Y/T be imposed.

However, one consideration that may indicate a need to limit the Y/T value is that a bridge is often constructed from a single heat of HPS70W. The reliability analysis assumes that the material properties in the structure are randomly distributed, so that there is an acceptably small risk that out-of-specification materials will happen to be located at locations of maximum demand. However, if the structure is constructed from one heat and that heat happened to have a high Y/T greater than the safe value, every cross section would be potentially affected by that high Y/T.

Presently, the Y/T of A992 steel is explicitly limited to 0.85. If a decision is made to put explicit limits on the Y/T for HPS70W or other steels in ASTM A709, the "safe" value may be considered as a specification limit on Y/T. For example, for HPS70W, the safe value of Y/T for HPS70W was 0.91. The data in Figure 3.1 and 3.2 show that there would be a significant percentage of present-day heats that would be rejected if this were required. Considering that the strength of the member is not in question if the Y/T exceeds the safe value, but rather only the ductility, and considering that the limiting Y/T for A992 is well above the safe value for that steel, a limiting Y/T value of 0.92 might be more appropriate than 0.91. Figure 3.2 shows that approximately 5% of present-day heats would be rejected with a Y/T limit of 0.92.

4.0 Recommendations and conclusions

4.1 Recommended specification changes

4.1.1 AISC Specifications

Since the revised recommendations for what was in Section B10 will now involve strength rather than just the cross section, it is appropriate to eliminate Section B10 and move to Sections F5, F6, and F7. Section F5 will have the new recommendations for holes in the tension flange. Section F6 should be entitled “HYBRID GIRDERS” and should contain the paragraph on hybrid girders. Section F7 should be entitled “FLANGES AND COVER PLATES” and should contain the rest of the text that was in Section B10. The note at the end of Section F1.1 should refer to section F5 rather than B10. Section F5 should read as follows:

F5. BEAMS WITH HOLES IN THE FLANGES

The major axis section properties for rolled or welded shapes, plate girders or cover-plated beams with holes in the compression flange may be computed using the gross section of the compression flange with no deduction for the holes if:

- the compression flange is composite with a concrete slab;
- the holes are standard size and contain the correct size bolts; or,
- the holes of any type comprise no more than 15% of the compression flange area.

The major axis section properties for rolled or welded shapes, plate girders or cover-plated beams with holes in the tension flange may be computed using the gross section of the tension flange with no deduction for the holes if:

$$F_u A_{fn} \geq Y_t F_y A_{fg} \qquad \text{(F5-1)}$$

where

A_{fg} = gross tension flange area, in.^{2} (mm^2)

A_{fn} = net tension flange area calculated in accordance with the provisions of Sections B1 and B2, in.^{2} (mm^2)

F_u = specified minimum tensile strength, ksi (MPa)

F_y = specified minimum yield strength, ksi (MPa)

Y_t = 1.0 for steel with $F_y \leq 50$ ksi (350 MPa)

= 1.1 otherwise

If $F_u A_{fn} < Y_t F_y A_{fg}$, the nominal flexural strength M_n at the location of the holes in the tension flange shall be determined as follows:

$$M_n = F_n S_x \qquad \text{(F5-2)}$$

where the nominal flexural stress F_n shall be determined as follows:

$$F_n = \frac{F_u A_{fn}}{Y_t A_{fg}} \qquad \text{(F5-3)}$$

The minor axis section properties for rolled or welded shapes, plate girders or cover-plated beams with holes in either flange may be computed using the gross section with no deduction for the holes if the holes in either flange comprise no more than 15% of the area of that flange.

4.1.2 AASHTO Specifications

Section 6.10.3.6 of the AASHTO LRFD Specifications should be changed to read as follows:

6.10.3.6 EFFECT OF HOLES IN THE FLANGES

The effect of holes in flanges shall be considered for the strength limit state but need not be considered for other limit states. The major axis section properties for flexural members with holes in the compression flange may be computed using the gross section of the compression flange with no deduction for the holes if:

- the compression flange is composite with a concrete slab;
- the holes are standard size and contain the correct size bolts; or,
- the holes of any type comprise no more than 15% of the compression flange area.

The major axis section properties for rolled or welded shapes, plate girders or cover-plated beams with holes in the tension flange may be computed using the gross section of the tension flange with no deduction for the holes if:

$$F_u A_{fn} \geq Y_t F_{yf} A_{fg} \qquad (6.10.3.6\text{-}1)$$

where

A_{fg} = gross tension flange area, in.^{2} (mm^2)

A_{fn} = net tension flange area as specified in Article 6.8.3, in.^{2} (mm^2)

F_u = specified minimum tensile strength of the flange specified in Table 6.4.1-1, ksi (MPa)

F_{yf} = specified minimum yield strength of the flange, ksi (MPa)

Y_t = 1.0 for steel with $F_y \leq 50$ ksi (350 MPa)

= 1.1 otherwise

If no deduction is required for the holes in either flange, the nominal flexural resistance may be determined using Sections 6.10.4.2.1 or 6.10.4.2.2 as applicable. If a deduction for the holes is required for the compression flange or if $F_u A_{fn} < Y_t F_{yf} A_{fg}$ for the tension flange, then the nominal flexural resistance shall be determined in accordance with Section 6.10.4.2.4. In this case, the nominal flexural resistance F_n for a tension flange if $F_u A_{fn} < Y_t F_{yf} A_{fg}$ shall be determined as specified in Section 6.10.4.2.4 but shall also be limited to:

$$F_n = \frac{F_u A_{fn}}{Y_t A_{fg}} \qquad (6.10.3.6\text{-}2)$$

If a deduction is required for holes in a compression flange Equation 2 shall also be used where $A_{fg}, A_{fn}, F_{u,,}$ F_{yf}, and Y_t are properties of the compression flange.

.

The minor axis section properties for flexural members with holes in either flange may be computed using the gross section with no deduction for the holes if the holes comprise no more than 15% of either flange area.

4.1.3 ASTM A709/AASHTO M270 Specifications

There were a few heats out of the more than 2400 heats of HPS70W that were examined that had Y/T of 0.98, and that is alarmingly high. However, there are occasional Y/T this high in Grade 50 steels as well. If the present design provisions or even the less conservative proposed design provisions are followed, the risk of these high Y/T causing premature necking or net-section fracture are acceptably small, therefore it could be argued that explicit specification limits on Y/T are not required. Furthermore, the risk is primarily that the ductility will be insufficient, the consequences of which are usually less problematic than the consequences of insufficient strength.

However, since the steel flange plates or tension members for an entire bridge may come from one heat, if that one heat happed to have a Y/T of 0.98, the risk of insufficient ductility of the overall bridge may be unacceptable. This might be a valid reason for imposing explicit specification limits on the Y/T. However, if limits arte considered, they should be considered for all bridge steels and not just HPS70W, since there is a risk of having high Y/T values in any Grade 50 steel as well. The benefit of imposing this limit must be balanced against the additional cost of the steel due to rejected heats. The “safe” upper-bound Y/T could be considered as a rational choice for the Y/T limit – in the case of HPS70W the safe Y/T was 0.91. One point greater or 0.92 would have a much lower impact in terms of rejected heats, and therefore would be a better choice.

4.2 Recommended future work

1. Additional wide plate tests should be performed to get results from additional heats of HPS70W and to investigate the effects of:
    - thicker plates
    - punched holes, plasma-punched holes, and flame-cut holes
    - increased hole density for the same $(A_n/A_g)/(Y/T)$ ratio
    - clamping force in bolted splices.

2. Additional girder tests should be performed to get some replication of the results, test additional heats of HPS70W, and to investigate:
    - the behavior of Grade 50 comparison tests
    - the behavior of girders fabricated from steel with an extreme Y/T of about 0.97
    - the effect of hybrid girders with an HPS70W tension flange and Grade 50 web
    - the effect of variation in web depth
    - the effect of four-point bending
    - the effect of a full bolted splice
    - whether limiting the stress in the tension flange to F_u gives a sufficiently small probability of net-section fracture, or whether the net section tress must be limited to 0.75 F_u as in a tension member; and,
    - if F_u on the net section is tolerable, whether the tension flange can continue to strain up to 2.5% after reaching a nominal stress on the net section equal to F_u so that the plastic moment on the net section can be attained

3. Analyses of these experiments should be performed to enhance interpretation of the results and to investigate the relationship between the ductility of a tension member and the rotational ductility of a plate girder.

4.2 Conclusions

1. HPS70W performed extremely well in both tension and flexural tests. In the flexural test, the girder reached the plastic moment capacity and continued to deform and increase in load capacity until lateral torsional buckling took place at moment of 110% of the plastic moment capacity, at 6.5% strain in the tension flange and 11% rotation (which corresponds to a rotational ductility of 3.87). Tensile and rotational ductility exceeded the minimum requirements and were comparable to the ductility of similar members fabricated with Grade 50 steel.
2. All grades of steel seem to behave in a similar manner such that the strength and ductility can be predicted on the basis of the parameter $(A_n/A_g)/(Y/T)$; i.e. the net-to-gross area ratio (A_n/A_g) divided by the yield-to-tensile ratio (Y/T). This parameter is equivalent to and can also be thought of as $(T\ A_n) / (Y\ A_g)$; i.e. the nominal net-section strength limit state $(T\ A_n)$ divided by the nominal gross-section yielding limit state $(Y\ A_g)$. In the wide-plate tests, gross-section yielding and adequate ductility (elongation greater than 10 times yield strain) was provided at $(A_n/A_g)/(Y/T)$ of 1.0 for all grades of steel.
3. In plots of elongation in the wide-plate tests vs. $(A_n/A_g)/(Y/T)$, the correlation of various steel grades was more consistent in terms of elongation than when the elongation was normalized by the yield strain, indicating that this way of normalizing tensile ductility may not be the appropriate, and that it may be better to characterize tensile ductility just in terms of elongation.

4. The behavior of tension members up to the point of failure can be predicted with reasonable accuracy using the shell finite elements.
5. The behavior of the flexural members up to the point of failure can be predicted with reasonable accuracy using a simple cross-sectional moment-curvature analysis.
6. Statistical analysis of the mill report tensile properties for more than 2400 heats of HPS70W revealed the mean Y/T was 0.84 and the coefficient of variation (COV) for the Y/T was 0.06, which is similar to the COV of A36 and various Grade 50 steels.
7. The present AISC and AASHTO provisions for tension members and for holes in flexural members would be conservative when applied to HPS70W or any other steel.
8. The present AISC and AASHTO provisions for flexural members with holes require a factor of 1.2 such that the ratio of A_n/A_g is greater than or equal to $1.2(F_y/F_u)$. The wide-plate experiments showed that adequate ductility was provided when A_n/A_g is greater than or equal to Y/T. These design provisions will result in adequate ductility when the Y/T is less than or equal to $1.2(F_y/F_u)$. This is almost always the case for all steels, so these provisions are conservative for all steels including HPS70W and even A514. However, these design provisions are excessively conservative and cause great difficulty in design. Furthermore, these design provisions result in varying levels of ductility for different steels since the relationship between the ratio of the minimum specified values (F_y/F_u).and the mean Y/T varies for each steel.
9. Alternative provisions for flexural members with holes were derived. The proposed provisions are based on a "safe" upper-bound Y/T with a probability of being exceeded about the same as the accepted probability of the yield strength being less than the minimum specified value (F_y). The statistical distribution of the Y/T for

many different grades of steel was examined, and it was found that for all Grade 50 steels the safe Y/T value was about equal to F_y/F_u, whereas for HPS70W and higher-strength A514 steel the safe Y/T was approximately $1.1(F_y/F_u)$. This distinction is reflected in the proposed design provisions.

5.0 References

AASHTO (1999), AASHTO LRFD Bridge Design Specifications, American Association of State Highway and Transportation Officials, Washington D.C

AISC (1998), Manual of Steel Construction, Load & Resistance Factor Design, Second Revision of the Second Edition, Chicago, Illinois

Beer, F. P., and Johnston, E. R., Mechanics of Materials, 2nd Edition, McGraw-Hill, New York, 1992, p. 367-371

Bartlett, F.M., R.J. Dexter, M.D. Graeser, J.J. Jelinek, B.J. Schmidt, and T.V. Galambos "Updating Standard Shape Material Properties Database for Design and Reliability", submitted to AISC Engineering Journal, Dec. 2001.

Brockenbrough, R. L., & Associates, "Effect of Yield-Tensile Ratio on Structural Behavior -– High-Performance Steels for Bridge Construction," Final Report to Naval Surface Warfare Center and Federal Highway Administration, March 1995

Dexter, R. J., Graeser, M., Saari, W. K., Pascoe, C., Gardner, C. A., and Galambos, T. V. (2000), "Structural shape material property survey," Technical report for Structural Shape Producers Council, University of Minnesota, Minneapolis, MN.

Dexter, R. J., and Ferrell, M., “Effects of weld metal strength and defects on the ductility of HSLA-100 plates.” Material Engineering Procedures, 14th International Conference on Offshore Mechanics and Arctic Engineering Conference, Salama et al., eds., Vol. III, ASME, New York, 1995, p. 449-454

Dexter, R.J. and M.L. Genrtilcore “Analysis of Plane Stress Ductile Fracture Propagation by Simulating Necking”, to appear in ASCE Journal of Structural Engineering, 2002.

Fisher, J.W., Galambos, T. V., Kulak, G.L., and Ravindra, M.K., “Load and Resistance Factor Design Criteria for Connectors”, Journal of the Structural Division, ASCE, Vol. 104, No. ST9, September, 1978.

Galambos, T. V., “Reliability of Connections, Joints, and Fasteners,” Structural Engineering Report No. 85-05, Washington University, St. Louis, MO, 1985.

Galambos, T. V., Hajjar, J. F., Earls, C. J., and Gross, J. L., “Required Properties of High-Performance Steels,” National Institute of Standards and Technology, Report No. 6004, May 1997

Green, P. S., The Inelastic Behavior of Flexural Members Fabricated from High Performance Steel, Ph.D. dissertation, Lehigh University, Bethlehem, PA, 2000

Kim, H. J., and Yura, J. A., “The effect of ultimate-to-yield ratio on the bearing strength of Bolted Connections,” Journal of Constructional Steel Research, Vol. 49, 1999, p. 255-269

Kulak, G. L., and Fisher, J. W., “Behavior of large A514 steel bolted joints,” ASCE J. Struct. Div., September 1969, p. 1873-1886

Lukey, A.F., and Adams ,P.F., “Rotation Capacity of Beams under Moment Gradient”, Journal of the Structural Division, ASCE, Vol. 95, No. ST6, June 1969

Mans, P., Yakel, A.J., and Azizinamini, A., "Full Scale Testing of Composite Plate Girders Constructed Using 70-ksi High Performance Steel," *Journal of Bridge Engineering*, ASCE, in press.

McDermott, J. F., “Plastic bending of A514 steel beams,” ASCE J. Struct. Div., September 1969, p. 1851-1871

Salmon, C. G., and Johnson, J. E., Steel Structures, Design and Behavior, 4th Edition, Harper Collins, New York, 1996, p. 73-75

Timoshenko, S., and MacCullough, G. H., Elements of Strength of Materials, 3rd Edition, D. Van Nostrand Company, New York, 1949

White, D. W., Barth, K. E., and Bobb, B. M., “Strength and Ductility of HPS70W Girders,” Georgia Institute of Technology Final Report to American Iron and Steel Institute, December 1998

Wright, W. J., Tjiang, H., and Albrecht, P., “Fracture Toughness of Structural Steels,” Final Technical Report to Federal Highway Administration Turner-Fairbank Highway Research Center, January 2001

Yakel, A. J., Mans, P., and Azizinamini, A., “Flexural Capacity of HPS70W Bridge Girders,” National Bridge Research Organization at the University of Nebraska Technical Report, November 1999